Author/s:
Miotto, PM;Yang, CH;Keenan, SN;De Nardo, W;Beddows, CA;Fidelito, G;Dodd, GT;Parker, BL;Hill, AF;Burton, PR;Loh, K;Watt, MJ

Title:
Liver-derived extracellular vesicles improve whole-body glycaemic control via inter-organ communication

Date:
2024-02-01

Citation:
Miotto, P. M., Yang, C. H., Keenan, S. N., De Nardo, W., Beddows, C. A., Fidelito, G., Dodd, G. T., Parker, B. L., Hill, A. F., Burton, P. R., Loh, K. & Watt, M. J. (2024). Liver-derived extracellular vesicles improve whole-body glycaemic control via inter-organ communication. Nature Metabolism, 6 (2), pp.254-272. https://doi.org/10.1038/s42255-023-00971-z.

Liver-derived extracellular vesicles improve whole-body glycemic control via inter-organ communication

Paula M. Miotto[1], Chieh-Hsin Yang[2], Stacey N. Keenan[1], William De Nardo[1], Cait A. Beddows[1], Gio Fidelito[1], Garron T. Dodd[1], Benjamin L. Parker[1], Andrew F. Hill[3], Paul R. Burton[4], Kim Loh[2,5], Matthew J. Watt[1*]

[1] Department of Anatomy and Physiology, School of Biomedical Sciences, Faculty of Medicine Dentistry and Health Sciences, University of Melbourne, Melbourne, VIC 3010, Australia.

[2] St. Vincent's Institute of Medical Research, Fitzroy, VIC, 3065, Australia

[3] Department of Biochemistry and Genetics, La Trobe Institute for Molecular Science, La Trobe University, Bundoora, Victoria, Australia

[4] Centre for Obesity Research and Education, Department of Surgery, Monash University, Melbourne, Victoria 3004, Australia.

[5] Department of Medicine, University of Melbourne, Fitzroy, VIC, 3065, Australia

*Correspondence to: Prof. Matthew Watt, Department of Anatomy and Physiology, School of Biomedical Sciences, Faculty of Medicine Dentistry and Health Sciences, The University of Melbourne, Victoria 3010, T: +61 3 8344 8663, Email: matt.watt@unimelb.edu.au

ABSTRACT

Small extracellular vesicles (EVs) are signalling messengers that regulate inter-tissue communication through delivery of their molecular cargo. Here, we show that liver-derived EVs are acute regulators of whole-body glycemic control in mice. Liver EV secretion into the circulation is increased in response to hyperglycemia, resulting in increased glucose effectiveness and insulin secretion through direct inter-organ EV signalling to skeletal muscle and the pancreas, respectively. This acute blood glucose lowering effect occurs in healthy and obese mice with non-alcoholic fatty liver disease (NAFLD), despite marked remodeling of the liver-derived EV proteome in obese mice. The EV-mediated blood glucose lowering effects were recapitulated by administration of liver EVs derived from humans with or without progressive NAFLD, suggesting broad functional conservation of liver EV signalling and potential therapeutic utility. Taken together, this work reveals a mechanism whereby liver EVs act on peripheral tissues via endocrine signalling to restore euglycemia in the post-prandial state.

Non-alcoholic fatty liver disease (NAFLD) is a common complication of obesity that encompasses a spectrum of liver disorders, including nonalcoholic fatty liver (NAFL, >5% liver fat accumulation) and the more progressive nonalcoholic steatohepatitis (NASH), which is histologically defined by steatosis, lobular inflammation, and hepatocyte ballooning [1]. NAFLD is closely associated with insulin resistance, dyslipidemia and an increased risk of type 2 diabetes and coronary heart disease, and progression to NASH increases the risk of fibrosis, cirrhosis, hepatic decompensation, and liver-related mortality [2]. It is estimated that ~25% of the world's population have NAFLD [3], and ~20% of NAFLD cases are classified as NASH. Strikingly, NAFLD incidence is ~75% in individuals with obesity [4] and 56% among patients with type 2 diabetes [5].

There is an incomplete understanding of the factors mediating the close relationship between NAFLD and diabetes, with the likelihood of multiple contributing factors, including hepatic insulin resistance and increased very low density lipoprotein secretion. NAFLD is also associated with the development of insulin resistance in peripheral tissues of obese patients, indicating that humoral factors secreted from the liver can impair insulin action in distant glucoregulatory tissues [6,7]. Indeed, the secretion of liver-derived proteins, which are known as hepatokines, is altered in NAFLD [8,9] and many hepatokines signal via autocrine/paracrine and endocrine signalling to induce changes in lipid metabolism, peripheral insulin action, and glycemic control [8-14]. These hepatokines are released from the liver via classical secretion, a process by which proteins that contain an N-terminus signal peptide are glycosylated within the endoplasmic reticulum and are transported to the Golgi apparatus within COPII-coated vesicles to the cell membrane, where they fuse and release proteins into the extracellular environment to signal to target cells [15]. While classical protein secretion is a hallmark of tissue communication, 80-90% of the proteins secreted by the liver do not contain a signal peptide [8,14], indicating that proteins secreted via alternative mechanisms are likely mediators of inter-tissue communication and metabolic control.

Small extracellular vesicles (EVs) are nanosized vesicles that contain lipids, proteins, and nucleic acid cargo that can be transferred to recipient cells and elicit functional responses [16]. Little is known regarding the role of liver derived EVs in regulating processes in other cells and tissues, and how the composition of EVs vary with progressive NAFLD. One study showed that chronic administration of EVs derived from isolated hepatocytes of mice with early-stage obesity promoted insulin sensitivity in recipient mice, and that these effects were ascribed to the actions of a single micro-RNA, miR-3075[17]. Conversely, hepatocyte EVs derived from mice with chronic obesity caused insulin resistance, possibly via proinflammatory activation in macrophages [17]. While this study

provided an important foundation in understanding how *chronic* treatment with hepatocyte EVs promotes tissue adaptations to impact blood glucose control, it is unknown whether the presence of EVs from other cells of the liver parenchyma impact these effects (e.g., Kupffer cells, hepatic stellate cells), whether such responses are altered during the progression from NAFL to early-stage NASH, and whether liver EVs activate acute cell signalling events and rapidly regulate metabolic responses in target tissues. In addition, recent work has shown that miRNAs are minor constituents of EVs and engineered fusogenic EVs carrying miRNA did not detectably alter the functionality of cells exposed to miRNA, indicating that other EV constituents, such as proteins, are likely to be important regulators of EV-mediated communication [18]. Given that EV production is influenced by hormone and nutrient availability [19], and EVs carry a variety of intracellular and integral membrane proteins, we hypothesised that liver-derived EVs are secreted in response to increased nutrient availability and exert acute functional changes in recipient cells to regulate metabolism.

In this study, we used mass-spectrometry proteomics to identify changes in the protein composition of liver-derived EVs during the transition from healthy liver to NAFL and NASH in mice. Irrespective of liver pathology, EVs derived from both mouse and human liver acutely improved glycemic control by increasing insulin secretion and improving glucose effectiveness, independent of changes in insulin sensitivity. These responses were specific to liver EVs and were dependent on the presence of EV transmembrane proteins. The secretion of liver EVs was enhanced by glucose availability in a healthy state, and suppressed in an insulin resistant state, indicating an important physiological role for liver-derived EVs to rapidly regulate glycemic control in response to fluctuating glucose levels.

Keywords (up to 10): glucose metabolism, insulin sensitivity, insulin secretion, extracellular vesicle, exosome, glucose effectiveness, non-alcoholic fatty liver disease

RESULTS

Small extracellular vesicle secretion with NAFLD progression

NAFLD and insulin resistance are common comorbidities, and factors secreted from liver are known to influence insulin action and glycemic control [10,17,20]. Accordingly, we hypothesized that the composition of liver derived EVs are altered in NAFL and NASH and that these EVs impair glycemic control in mice. We first validated the mouse models of diet induced NAFL and NASH. Body weight, liver, and epididymal adipose tissue mass were increased in mice fed a NASH and NAFL diet relative to Control fed mice (Extended data **Fig. 1A-B**). Mice fed the NAFL diet

were profoundly glucose intolerant (Extended data **Fig. 1C-D**) and hyperinsulinemic (Extended data **Fig. 1E**) compared to mice fed the Control and NASH diet. Mice fed the NASH diet had significantly elevated liver and adipose tissue mass (Extended data **Fig. 1B**) and were glucose intolerant and hyperinsulinemic (Extended data **Fig. 1C-E**) compared to Control mice.

Histopathology on thin liver sections revealed hepatic steatosis in NAFL and NASH (**Fig. 1A**) and biochemical assessment confirmed that liver triglyceride levels were increased ~5-fold in NAFL and NASH compared with Control mice (**Fig. 1B**). The NAFLD activity score (NAS) [21 22] was increased in NAFL compared with Control and was further increased in NASH (**Fig. 1C**), primarily due to an increase in hepatocyte ballooning (**Fig. S1F-H**)**.** Serum alanine aminotransferase (ALT) is a marker of liver damage and was higher in NAFL and NASH compared with Control mice (**Fig. 1D**). Fibrosis is a feature of progressive NAFLD and while there was an upregulation of several pro-fibrotic genes in the liver from NASH mice (e.g., *Tgf1β, Timp1, Cd11*; **Fig. 1E**), there was no significant histologically confirmed fibrosis in either NAFL or NASH mice (**Fig. 1A**). Collectively, these models recapitulate features of NAFL and early-stage NASH without significant fibrosis.

To determine the impact of NAFLD on liver EV secretion, livers were excised from mice and 300 μm precision-cut slices were prepared and incubated in an oxygenated, nutrient rich buffer, as described by our lab previously [9,23]. Given the potential for liver damage and stress, the ATP / ADP ratio of liver slices and snap frozen whole liver from donor mice was assessed. This was not different between groups, indicating viability of the liver slices (Extended data **Fig. 1I**). Liver-secreted factors were collected after 16 h incubation and EVs were isolated and purified using a differential centrifugation technique. Nanoparticle tracking analysis (NTA) showed that the majority of the EVs were of the expected size (~130 nm, **Fig. 1F**)[24], and cryo-electron microscopy showed that the EVs exhibited the characteristic EV morphology, consisting of a lipid bilayer and spherical structure (**Fig. 1G**). The presence of validated EV proteins, including TSG101, CD63, CD9, HSP70, and CD81 were confirmed by immunoblot analysis (**Fig. 1H**). Purity of the EVs was further confirmed by the absence of calnexin, a protein specifically localized to the endoplasmic reticulum (**Fig. 1H**). Lipoproteins can co-purify with EVs and were present, but barely detectable, in the isolated EV preparation (4 of 1779 EV proteins detected by mass spectrometry, including apoC-III, ApoA-I, Apo-E, and LSR, **Table S1**). Proteins denoted as ‘classically’ secreted are known to associate with EVs and ~5% of the proteins in liver EVs contained a N-terminal signal peptide (**Table S1**). The

EVs were almost devoid of endotoxin contamination, with levels ~50-fold lower than that detected in the serum of mice (Extended data **Fig. 1J**).

The impact of NAFL and NASH on liver EV secretion was determined by examining the concentration of secreted EVs and the total protein contained within the EVs secreted from liver slices. NTA analysis demonstrated an increase in the concentration of EVs secreted from the livers of NASH mice compared with NAFL and Control (**Fig. 1I**). The protein abundance within the secreted EVs was lower in NAFL and NASH compared with Control when normalised per mg liver slice (**Fig. 1J**), however, when total liver mass was considered, the amount of protein in secreted EVs was similar between experimental groups (**Fig. 1K**). Together, these data demonstrate that EV secretion is increased in NAFL and NASH, but the total protein cargo within the secreted EVs is similar to Control.

The liver secreted EV proteome is altered in NAFL and NASH

The composition of EVs derived from tissues other than liver are altered in many disease states [25-28]. Using LC-MS/MS proteomics, we identified 1779 proteins that were contained in liver EVs, and 1688 were common to all groups (**Fig. 2A**). The differences in the EV proteome between Control and NAFL/NASH groups was captured by principal component analysis (**Fig. 2B**). Mice with NAFL secreted EVs that contained 91 upregulated proteins and 66 downregulated proteins compared with Control (**Fig. 2C, Table S1**), while 222 proteins were increased, and 249 proteins were decreased in liver derived EVs from NASH mice compared with Control mice (**Fig. 2D, Table S2**). Notably, there were no differences between NAFL and NASH fed mice (**Fig. 2E**), indicating that changes in liver EV protein composition is an early manifestation of NAFLD progression.

Pathways enrichment analysis of the 'top 20 processes regulated' indicated that EV proteins from NAFL and NASH are associated with upregulation of carbohydrate metabolism and small molecule catabolic process, and downregulation of fatty acid metabolism via mitochondrial β-oxidation and ATP-dependent activity (Extended data **Fig. 2A-B**). Further analysis showed that NAFL and NASH EVs contained proteins implicated in the upregulation of glycolysis and gluconeogenesis, glycogen metabolism, pyruvate metabolism, and the tricarboxylic acid (TCA) cycle, and downregulation of lipid processes including lipid transport, elongation, synthesis, and oxidation (**Fig. 2F-G**). Further interrogation using Ingenuity Pathway Analysis of 'diseases and functions' highlighted that proteins within liver EVs from NAFL or NASH mice are associated with greater 'hepatic steatosis', 'hyperlipidemia', and

'cell death of cancerous cells', and lower 'quantity of hepatocytes', 'ATP synthesis', and surprisingly, 'fibrogenesis' (Extended data **Fig. 2C-D)**. Together, these data highlight that the liver EV proteome is altered in NAFLD and that these proteins predict upregulation of various pathways of carbohydrate metabolism.

Liver EVs increase glucose tolerance and insulin secretion

Given the pronounced changes in the liver EVs proteome with NAFL and NASH, and the association of these proteins with altered carbohydrate metabolism, we examined the effects of liver secreted EVs on glycemic control. In all experiments, EVs were administered to mice 1 h prior to metabolic assessments via i.p or i.v injection at a dose of 30 µg EV protein, which is an amount commonly used in previous *in vivo* studies [20,29-32]. A cross-over design was implemented to test the effects of liver EVs derived from NAFL or NASH mice in lean normoglycemic mice and EVs secreted from healthy control mice in recipient mice with NAFL or NASH. Surprisingly, liver secreted EVs, regardless of the donor, greatly improved whole-body glycemic control in all mice. This was reflected by reduced blood glucose levels following an oral glucose challenge resulting in an ~40% reduction in the glucose area under the curve in Control, NAFL and NASH mice that received liver-secreted EVs (**Fig. 3A-C;** Extended data **Fig. 3A-C**). This response was conserved in Control female mice that received an i.p injection of liver derived EVs (Extended data **Fig. 3D**). We also examined the effects of intravenous (i.v) administration of liver derived EVs and observed marked improvements in glycemic control that recapitulated responses seen with i.p administration (Extended data **Fig. 3E**). The improvement in glycemic control was accompanied by an ~2-fold increase in serum insulin concentrations in response to a glucose bolus following i.p or i.v injection of liver EVs (**Fig. 3D-F;** Extended data **Fig. 3F**), regardless of the EV donor or recipient. To determine whether these effects were specific to liver secreted EVs or EVs in general, we conducted oral glucose tolerance tests in mice that were administered empty liposomes, adipose secreted EVs, or serum derived EVs. Glucose tolerance (Extended data **Fig. 3G-I**) and serum insulin levels (Extended data **Fig. 3J**) were not different between groups, indicating specific actions of liver secreted EVs in regulating glycemic control.

Glucose-sensing by the liver increases liver EV secretion

Given that liver EV administration improved glycemic control under glucose-stimulated, but not basal states, we proposed that hyperglycemia stimulates the secretion of EVs from the liver. To test this, liver slices from healthy mice were treated with low (2 mM) or high (20 mM) glucose, in the presence or absence of the powerful glucoregulatory hormones insulin (10 nM), glucagon (20 pg/ml) or norepinephrine (15 pg/ml), and EVs were

collected from the incubation medium. Secreted liver EV particle concentration and the total EV protein cargo load was increased with high glucose (**Fig. 3G-H**), and none of the glucoregulatory hormones influenced liver EV secretion under high glucose stimulation (Extended data **Fig. 3K-L**). Proteomics analysis showed that the liver EV proteome was not different between low and high glucose conditions (Extended data **Fig. 3M, Table S3),** highlighting an increase in EV release with high glucose in the absence of changes to protein composition. To determine whether these observations in isolated liver were recapitulated in vivo, we assessed the amount of liver derived EVs in serum of Control mice in the fasted state and after oral glucose administration. Imaging flow cytometry analysis was used to identify the presence of canonical EV markers (i.e., CD9, CD63) and liver EVs were identified by co-staining with the liver-specific protein asialoglycoprotein 1 (ASGPR1; gene name: *Asgr1*) [33] (**Table S1**). The number of liver-derived EVs was increased in the serum of healthy Control mice following glucose administration when compared with fasted mice (**Fig. 3I-J;** Extended data **Fig. 3N-Q)**. In contrast, NAFL mice were resistant to glucose-stimulated EV secretion from the liver (**Fig. 3K;** Extended data **Fig. 4A-D**). Together, these data show that the liver increases EV secretion after sensing an increase in glucose availability, and that resistance to glucose-stimulated EV secretion is a feature of NAFL and glucose intolerance.

Intact liver EVs are required for improved glycemic control

EVs contain a variety of proteins, lipids, and nucleic acids that can influence cell function when delivered to recipient cells. To determine whether the EV constituents alone are sufficient to improve glycemic control, we next disrupted the EV structure by sonication prior to injecting into mice. Sonication of EVs did not influence glycemic control (**Fig. 3L;** Extended data **Fig. 4E**) or insulin secretion (**Fig. 3M**) in Control or NAFL mice, demonstrating that liver EVs must be intact for their biologically active constituents to induce glycemic effects (**Fig. 3A-C**). Further, cell receptor proteins are important mediators of EV-target cell interactions through receptor-ligand binding, fusion, or endocytosis [34]. 'Shaving' EV surface proteins through mild proteinase K digestion [35] blunted the EV-mediated improvements in glycemic control (**Fig. 3N and P;** Extended data **Fig. 4F and G**) as well as the rise in serum insulin levels (**Fig. 3O and Q**) in both control and NAFL mice. 'Shaving' the EV surface proteins did not alter the morphology (Extended data **Fig. 4H**) or size (Extended data **Fig. 4I**) of the EVs. Hence, EV surface proteins are required for the full effects of liver EVs to increase insulin secretion and improve glycemic control in mice.

The brain regulates blood glucose levels through neural suppression of hepatic glucose output, enhanced insulin secretion, and increased skeletal muscle glucose uptake [36]. EVs from adipose-derived stem cells communicate

with microglia within the brain [37], raising the possibility that liver-derived EVs could influence glycemic control via direct action in the brain. To test this possibility, we performed intracerebroventricular (ICV) injections of either saline or NAFL liver EVs (16 µg, 1-3 h prior to GTT) directly into the central ventricular system. Liver-derived EVs administered directly into the brain did not alter glycemic control (Extended data **Fig. 4J**) or serum insulin levels when compared with saline (Extended data **Fig. 4K**), indicating that liver-derived EVs exert effects on glycemic control and insulin secretion through direct engagement with peripheral tissues.

Liver-secreted EVs do not regulate insulin sensitivity

As chronic administration of hepatocyte derived EVs improves peripheral insulin action [17], we anticipated that the blood glucose lowering effects of acute liver EVs would be mediated by enhanced insulin sensitivity. Unexpectedly, liver-secreted EVs did not alter whole body glycemic responses in control mice or mice with NAFL following i.p administration of insulin (**Fig. 4A-B**). Further experiments conducted in isolated tissues *ex vivo* confirmed that liver-derived EVs do not impact hepatic glucose output in Control mice (**Fig. 4C**) or glucose uptake into isolated skeletal muscle or white or brown adipose tissues under basal or insulin-stimulated conditions in Control or NAFL mice (**Fig. 4D-F;** Extended data **Fig. 4L-N**). These findings were further supported by assessment of insulin sensitivity in Control mice using hyperinsulinemic-euglycemic clamps. Mice that received saline or NAFL EVs had similar basal and clamped glucose concentrations (Extended data **Fig. 4O**) and plasma insulin levels were elevated in all mice during the clamp (Extended data **Fig. 4P**). The glucose infusion rate during the clamp (**Fig. 4G**), which reflects whole-body insulin sensitivity, was not different between groups. Collectively, these independent experiments demonstrate that liver secreted EVs do not acutely improve glycemic control by enhancing insulin sensitivity.

Liver EVs enhance glucose effectiveness in skeletal muscle

Glycemic control is regulated by several factors, including glucose effectiveness (G_E), which is defined as the effect of an acute increase in glucose concentrations to facilitate its own metabolism and can account for ~45-65% of glucose disposal in humans [38]. Having demonstrated that liver derived EVs do not impact insulin sensitivity, we next asked whether EVs modulate G_E, and directly tested this by examining glycemic control in a short-term model of insulin deficiency. Mice were treated with low dose streptozotocin (STZ; 40 mg / kg) to induce insulin deficiency 2 weeks prior to glucose tolerance testing. While STZ treated mice were severely glucose intolerant compared to healthy control mice, a single dose of Control liver secreted EVs administered 1 h prior to an oral GTT dramatically

improved glycemic control (**Fig. 5A;** Extended data **Fig. 5A**) despite insulin deficiency and the absence of glucose-stimulated insulin secretion (**Fig. 5B**). Liver EVs derived from Control or NAFL mice also improved glycemic control after intraperitoneal injection of glucose in both healthy and insulin resistant mice (**Fig. 5C-D**), an experimental approach used to bypass incretin effects and insulin secretion [39]. Together, these data indicated that liver EVs improve glycemic control by increasing glucose effectiveness.

To further address this possibility, whole-body substrate oxidation and energy expenditure in Control mice were evaluated in the absence or presence of liver derived EVs from NAFL mice. Carbohydrate oxidation (**Fig. 5E**) was increased >2-fold within 2 hours of liver EV administration, independent of changes in fat oxidation (Extended data **Fig. 5B**), increased energy expenditure (Extended data **Fig. 5C**), and similar physical activity (Extended data **Fig. 5D**). We next examined the effect of NAFL derived EVs to directly increase G_E in skeletal muscle using established EV concentrations for ex vivo analyses [30,40-42]. Liver-derived EVs (10 µg/ml) increased glucose uptake in the presence of high, but not low or moderate, 2-deoxyglucose (2-DG) concentrations in fully differentiated C2C12 myotubes (**Fig. 5F**), and these effects were recapitulated in separate experiments conducted in isolated mouse soleus muscles (**Fig. 5G**). Together, data derived from several independent models demonstrate that liver derived EVs directly promote glucose effectiveness in skeletal muscle, independent of the effects of insulin secretion by the pancreas or other endocrine factors.

To identify a mechanism for enhanced glucose effectiveness with liver EVs, we repeated studies in STZ treated mice and focussed on GLUT4 translocation in skeletal muscle. Mice were injected with either saline or control liver EVs (30 µg) then gavaged with water (vehicle) or glucose (2 g/kg) one hour later. There was no evidence of glucose-stimulated insulin secretion, confirming the veracity of this model (Extended data **Fig. 5E**). Mice treated with liver EVs and glucose had greater abundance of GLUT4 protein at the plasma membrane (**Fig. 5H**) and a corresponding reduction in microsomal GLUT4 protein (**Fig. 5I**) when compared with mice treated with vehicle or glucose. There was no difference in plasma membrane caveolin 3 content between groups (**Fig. 5H** and Extended data **Fig. 5F**). These data indicate that liver EVs increase plasma membrane GLUT4 translocation to enhance glucose effectiveness in skeletal muscle.

Liver EVs regulate cell signalling in skeletal muscle

To gain insights into possible upstream regulators of liver EV-mediated glucose effectiveness, we evaluated the phosphoproteomic profile of isolated soleus muscles incubated in low or high glucose, and high glucose with liver EVs (10 µg/ml) from NAFL mice. In total, we quantified 13,140 phosphosites in 2,247 proteins. High glucose stimulation resulted in the up- and down-regulation of 27 and 23 phosphosites, respectively, when compared to low glucose ($q<0.05$) (**Fig. 6A, Table S4)**. Exposure to liver EVs from NAFL mice in the presence of high glucose resulted in the up- and down-regulation of 61 and 48 phosphosites, respectively, when compared to high glucose alone ($q<0.05$) (**Fig. 6B, Table S5**). This included increased phosphorylation of the protein STIM1 (S524), a regulator of calcium homeostasis, that is phosphorylated with feeding in mouse liver [43], supporting a possible role in regulating glucose effectiveness. No single phosphorylation site regulated by high glucose was further regulated by liver EVs, indicating that glucose-dependent and independent pathways likely synergize to mediate EV effects on glucose effectiveness. This lack of commonality in signalling between conditions was highlighted by pathway analysis of 'biological processes', where there was minimal overlap between the high glucose conditions in the absence (Extended data **Fig. 5G**) or presence (Extended data **Fig. 5H**) of liver EVs. There were proteins regulated by both high glucose and EVs, but notably, regulation occurred at different phosphorylation sites (**Fig. 6C-D**)**.** This included downregulation of phosphosites in the proteins PROB1 (S396, S407, S398, S451) and TNS1 (S1427, S963) and upregulation of phosphosites in NACA (S1914, S1491), CAMK2b (S397, T400), and PDHA1 (S295, S300). Both CAMK2b and PDHA1 are known regulators of glucose uptake and oxidation [44], respectively, supporting a possible involvement of these proteins in mediating glucose effectiveness.

Bioinformatic analysis indicated that calcium-sensitive pathways were activated in skeletal muscle in response to high glucose (Extended data **Fig. 5G**) and that liver EVs further activated a variety of signalling events associated with calcium, including the serine/threonine-specific protein kinase CaMKII. Accordingly, we suppressed calcium release from the sarcoplasmic reticulum with dantrolene and prevented CaMKII activity with the cell permeable inhibitor KN-62, followed by assessment of EV-mediated G_E. The EV-mediated increase in glucose uptake under hyperglycemic conditions (**Fig. 5F-G**) was completely ablated with dantrolene and KN-62 in isolated murine skeletal muscles (**Fig. 6E-F**). Notably, there was no effect of either compound on glucose uptake under low or high glucose conditions (without EVs), showing specificity of this response (Extended data **Fig. 5I**). Further, the EV-mediated increase in glucose uptake was also abolished with dantrolene and KN62 in C2C12 myotubes (**Fig. 6G-H**). Collectively, these data demonstrate direct and divergent signalling in response to high glucose and liver

EVs, and the requirement of sarcoplasmic reticulum calcium release and activation of CaMKII for EV-mediated G_E.

Liver EVs directly stimulate GSIS in primary islets

Given the effects of liver derived EVs on insulin secretion in mice, we next asked whether EVs increase GSIS by direct actions on the pancreas. In agreement with the *in vivo* studies showing increased GSIS with liver EVs (**Fig. 3D-F**), acute exposure of isolated murine pancreatic islets to NAFL liver EVs (10 µg/ml) increased insulin secretion 2-fold when exposed to high glucose but not low glucose (**Fig. 7A**). This response was completely attenuated when islets were exposed to EVs treated with proteinase K, highlighting the importance of EV transmembrane proteins in regulating direct liver EV-islet interactions and insulin secretion (**Fig. 7A**).

To examine the possible mechanisms that underpin the increase in GSIS with liver EVs, we systematically examined key aspects of the insulin secretion pathway (**Fig. 7B**). Glucose oxidation and the subsequent rise in ATP / ADP ratio are key events in K^+ channel inhibition and insulin secretion. Liver EVs acutely increased glucose oxidation by 1.9-fold in the presence of high glucose, but not low glucose (**Fig. 7C)**, but surprisingly, this did not increase the ATP / ADP ratio (**Fig. 7D**). In separate experiments, addition of liver EVs to islets did not affect insulin secretion from islets treated with tolbutamide (K^+ channel inhibitor that increases insulin secretion) or diazoxide (K^+ channel activator that suppress insulin secretion) (**Fig. 7E-F,** Extended data **Fig.6A-B**), suggesting an ATP independent event. Liver EVs retained their ability to enhance GSIS in the presence of secretagogues that target cellular depolarisation events downstream and independent of the K^+ channel. This included arginine to increase depolarisation of the plasma membrane (**Fig. 7G;** Extended data **Fig.6C**) and alanine to activate the voltage sensitive calcium change downstream of the K^+ channel (**Fig. 7H;** Extended data **Fig. 6D**). These effects could be explained by known actions of metabolic signals responsive to glucose metabolism on vesicle “priming” and exocytosis [45]. We also tested liver EV effects in islets treated with Exendin-4 to activate GLP-1-dependent insulin secretion via cAMP. Liver EVs increased GLP-1-dependent insulin secretion (**Fig. 7I;** Extended data **Fig. 6E**), which further supports the likelihood of independent metabolic effects mediated by liver EVs under high glucose conditions. The cellular insulin content was not notably different between conditions in any experiment (Extended data **Fig. 6F-J**), demonstrating collectively unaltered packaging or production of insulin in response to liver EVs. Altogether, these experiments show that liver EVs acutely and directly potentiate GSIS in islets isolated from mice via a mode of action involving increased glucose oxidation.

Human liver derived EVs improve glycemic control

We next examined the potential translational relevance of liver secreted EVs in regulating glycemic control. Liver wedges were procured from patients undergoing bariatric surgery for obesity treatment, liver slices were prepared, and EVs were collected and purified as described for mice (**Fig. 8A**). Of the 19 recruited patients, 8 had no liver pathology, 8 had NAFL, and 3 were diagnosed with NASH (Extended data **Table 1**). NTA analysis revealed similar rates of EV secretion between groups (**Fig. 8B**). Next, saline or human-derived liver EVs were injected i.p into mice with severe combined immunodeficiency (SCID) 1 hour prior to an oral glucose tolerance test. SCID mice lacking T and B cells do not reject human biological substances [46] and have been validated for metabolic studies [47]. EVs from patients with similar histopathology were combined to attain sufficient material for in vivo analysis (i.e., 2-3 donors per n=1 injection into mice). Administration of human liver-secreted EVs obtained from Healthy or NAFL donors improved glycemic control in mice (**Fig. 8C**) and this was accompanied by an increase in plasma insulin levels following glucose administration, but not in the basal state (**Fig. 8D**). These data align with experiments using mouse derived liver EVs (**Fig. 3A-F**) and demonstrate a conserved effect of liver EVs to improve glycemic control and increase insulin secretion during hyperglycemia.

DISCUSSION

EVs are important signalling messengers that regulate intercellular and inter-tissue communication through delivery of their molecular cargo [16]. EVs are also implicated in the pathogenesis of several diseases, including obesity and type 2 diabetes, and these effects have mostly been ascribed to distinct miRNAs contained within EVs derived from cells within hypertrophic adipose tissue [16,30,48]. In the current study, we demonstrate a role for liver secreted EVs as acute and powerful regulators of glycemic control. We demonstrate the existence of an unanticipated negative feedback mechanism, whereby liver sensing of increased blood glucose levels enhances liver EV secretion, which in turn are delivered to skeletal muscle and pancreas to synchronously increase glucose effectiveness and insulin secretion, respectively. This profound blood glucose lowering effect was apparent in healthy mice and those with NAFL and NASH, and was recapitulated by administration of liver EVs derived from humans without or with NAFLD, suggesting broad conservation of liver EV signalling, irrespective of disease state.

EV secretion is regulated in response to acute stimuli and in diseased states. Our data showing increased liver EV secretion in response to hyperglycemia, both in isolated liver slices and in mice *in vivo*, extends on previous findings reporting nutrient-driven EV secretion in a variety of cultured cell types including hepatocytes [49,50], adipocytes [51], monocytes [52], and endothelial cells [53]. While many factors are likely to regulate EV secretion, together, these data demonstrate a mechanism whereby acute increases in blood glucose are sensed by the liver, which results in enhanced EV secretion. Our data further align with the clinical observation in type 2 diabetes and NASH patients of concomitant increases in circulating EV levels and higher blood glucose levels [54-56], and conversely, reduced circulating EVs and fasting glucose levels in individuals with obesity following bariatric surgery [57]. It is noted that the circulating EV pool is the product of EV secretion from various tissues, and an exclusive role for liver EVs cannot be directly inferred from these clinical studies, however, our findings in mice indicate that liver EVs would likely contribute to this pool.

There is emerging evidence that EVs, particularly those derived from adipose tissue, are functional vectors that regulate metabolism in a variety of tissues through transfer of specific miRNAs to recipient tissues [20,30,48,51,58-60]. Findings from the present studies extend our knowledge of the physiological role of EVs by demonstrating a powerful and rapid effect of liver derived EVs on glycemic control. Liver derived EVs do not impact insulin sensitivity acutely and several lines of evidence using distinct methodologies demonstrate that the blood glucose lowering effects of liver EVs are mediated by (1) enhanced glucose effectiveness and increased glucose oxidation in skeletal muscle, which involves increased GLUT4 translocation to the plasma membrane and is dependent on calcium release from the sarcoplasmic reticulum and CaMKII activation; and (2) increased GSIS by the pancreas. These effects are only observed under hyperglycemic conditions, are conserved in isolated muscle and pancreatic islet preparations, but not following administration to the brain, and were not observed when mice were injected with liposomes or EVs from adipose tissue or serum. Taken together, these data indicate a mechanism whereby liver EVs act directly on peripheral tissues to restore euglycemia in the post-prandial state.

Proteomic evaluation of the EVs revealed the presence of ~1780 proteins and we determined that the rapid effects of liver EVs on glycemic control are primarily dependent on the presence of transmembrane proteins contained within liver EVs. While our phosphoproteomic data strongly implicate protein-mediated signalling as an essential component of liver EV metabolic effects, most notably in skeletal muscle, further work is needed to determine the precise EV proteins mediating these beneficial effects on glycemic control and whether these proteins exert their

actions via receptor-ligand effects and/or endocytosis. In addition, nucleic acids and lipids contained within EVs have been shown to regulate metabolism and a role for these molecules in blood glucose control cannot be discounted. Nevertheless, the discovery of liver derived EVs as potent regulators of glycemic control has provided new insights into inter-tissue communication and for future therapeutic opportunities targeting liver EVs. It is noted that the liver is composed of several cell types (e.g., hepatocytes, Kupffer cells, hepatic stellate cells) and further studies are required to delineate the effects of EVs produced from specific cell type/s in mediating effects on glycemic control.

Communication between the pancreas and liver plays an essential role in regulating glycemic control, where glucose sensing by the pancreas alters insulin and glucagon secretion to regulate hepatic glucose production [61]. More recent evidence demonstrates alternative endocrine communication between the liver and pancreas, where classically secreted hepatokines were shown to regulate insulin secretion [62]. Our work provides an advance in the understanding of liver-pancreas communication by establishing that liver secreted EVs increase GSIS from islets by increasing glucose oxidation, independent of the effects of incretins and other endocrine factors, as demonstrated during the i.p GTT and studies in isolated islets. The increase in GSIS was not mediated by changes in the ATP/ADP ratio and was independent of effects on the K^+ channel and other downstream regulatory points in the insulin secretory pathway. Changes in metabolites and / or signalling molecules associated with increased glucose oxidation are likely regulators, including mitochondrial reactive oxygen species production, the NADPH/$NADP^+$ ratio, and anaplerotic metabolism of pyruvate to tricarboxylic acid cycle intermediates such as oxaloacetate or malate [45].

NAFLD is closely linked to type 2 diabetes and the factors regulating this close relationship remain incompletely defined. Previous studies have shown that classically secreted proteins are altered in murine NAFL / NASH and that these proteins regulate insulin sensitivity, lipid metabolism and inflammation in recipient cells and tissues [8-14]. Given that approximately 90% of proteins secreted by the liver are contained in vesicles [8], we surmised that EVs secreted from livers of NAFL/NASH donors would induce metabolic dysregulation in recipient tissues and impair glycemic control in lean healthy recipient mice. This possibility was supported by marked changes in the EV proteome in NAFL and NASH when compared to EVs from healthy mice. Contrary to our hypothesis, acute administration of liver EVs from mice with a healthy liver or mice with NAFL or NASH markedly improved glycemic control in all recipient mice. Moreover, this finding was recapitulated in studies examining effects of EVs derived

from human donors with healthy livers or progressive NAFLD. These findings do not concur with recent work examining effects of hepatocyte secreted EVs on glycemic control. Ji *et al*. reported insulin sensitizing effects of hepatocyte derived EVs from mice with early onset obesity, and presumably mild NAFL, and reversal of these effects in chronic obesity, and presumably more advanced NAFLD, where isolated hepatocytes secrete EVs that cause insulin resistance secondary to tissue inflammation [17]. Moreover, EVs from obese mice decreased glucose tolerance in lean mice but were without effect when given to obese mice, but in obese mice, EVs from lean mice improved insulin sensitivity.

While it is difficult to reconcile the current findings and those of Ji *et al* into a coherent model, it is noted that there are important differences between studies including the EV source (liver slices vs. cultured primary hepatocytes), duration of dietary intervention (>20 weeks vs 4 and 16 weeks), route of EV administration (i.p vs. i.v) and frequency of EV administration (single vs. twice/week for 4 weeks). Given the complexity of the molecular cargo in liver EVs, it is probable that acute and prolonged exposure to EVs will induce differing responses in tissues (i.e., signalling versus metabolic adaptation) and that these effects may extend to the regulation of other cellular processes, as has been shown by others [63].

In conclusion, these data identify an unanticipated mode of inter-tissue communication where liver EVs are secreted in response to hyperglycemia and rapidly restore euglycemia by increasing insulin secretion from the pancreas and glucose effectiveness in skeletal muscle. These insights have several implications for future investigation and potential translational relevance. First, the results indicate that selectively enhancing liver EV secretion may represent a potential therapeutic strategy for conditions of impaired glucose metabolism. Second, the results reinforce the importance of glucose effectiveness in skeletal muscle for the maintenance of blood glucose, and we propose the use of liver EVs as an investigative tool to unravel potential therapeutic targets for conditions of impaired glycemic control. Future work will build on the phosphoproteomics data presented herein to determine liver EV-induced signalling and how this can be harnessed for pharmacological intervention in type 2 diabetes.

METHODS

Study approval

All animal procedures were done in accordance with the guidelines for the care and use of laboratory animals and approved by the Animal Welfare and Ethics Committee at the University of Melbourne (AEC 1814403, 1814363,

20063, 22305, 10324). Mice were housed in the Biomedical Science Animal Facility at the University of Melbourne, maintained on a 12 hr:12 hr light/dark cycle at 22-24°C and 40-60% humidity, with free access to food and water. Collection of human tissues were done in accordance with human ethics at the University of Melbourne (ID 1851533) and approved by The Avenue Hospital Human Research Ethics Committee (ID WD00006) and the Alfred Hospital Human Research Ethics Committee (ID GO00005).

Mice

Male C57BL/6J mice (12-15 weeks old; JAX 000664) were randomised to a control (SF13-081, Specialty Feeds, Western Australia, 12% energy from lipids (23 g/kg lard, 29 g/kg soy bean oil), 25.8% protein, 62.2% carbohydrate (201 g/kg sucrose)), high-fat (NAFL, SF04-001, Specialty Feeds, 43% energy from lipids (207 g/kg lard, 29 g/kg soy bean oil; 10% saturated, 5.8% palmitic acid), 21% protein, 37% carbohydrate (201 g/kg sucrose), or high fat-high fructose + 2% cholesterol diet (SF16-033, Specialty Feeds, NASH, 39.8% energy from lipids (172 g/kg lard, 28 g/kg soy bean oil), 20% protein, 40.2% carbohydrate (107 g/kg sucrose, 222 g/kg fructose) for 20 weeks. Mice were anesthetized using sodium pentobarbitol (60 mg / kg) and killed using cervical dislocation. Blood, liver, skeletal muscle, epididymal, or brown adipose tissue were collected for EV secretion or metabolism experiments. Separate cohorts of male C57BL/6J mice fed the 3 different diets for 20 weeks (matched for body weight prior to EV injection studies) or female C57BL/6J mice were used for functional studies. Severe combined immunodeficient mice (SCID; ~10 weeks old; JAX001303) were purchased from the Animal Resource Centre (ARC) and maintained on a standard chow diet for ~1 week before experiments.

STZ treatment

Male C57BL/6J mice (12-15 weeks old, JAX 000664) were injected with streptozotocin (40 mg / kg, Sigma Aldrich, cat# S0130) diluted in citrate buffer or citrate buffer alone for 5 consecutive days [64] before functional experiments (described below).

Human patients

Collection of human tissues were done in accordance with human ethics at the University of Melbourne (ID 1851533) and approved by The Avenue Hospital Human Research Ethics Committee (ID WD00006) and the Alfred Hospital Human Research Ethics Committee (ID GO00005). Patients with obesity undergoing bariatric surgery consented in writing to participate. This was a prospective study, and therefore sex and gender were not

considered. Exclusion criteria involved: <18 year of age, excessive alcohol use, evidence of other liver disease including viral hepatitis, cirrhosis, autoimmune hepatitis, and hyperthyroidism. Clinical details including metabolic comorbidities, body weight, height, medications, and medical history were collected using a questionnaire, and fasting blood was measured for alanine aminotransferase, bilirubin, triglycerides, and HOMA-IR. A 1 cm^3 wedge biopsy was collected, and precision cut liver slices were prepared as described below.

Histological analysis

Liver tissue obtained from mice or humans were fixed in formalin, sectioned and stained with hematoxylin and eosin or Masson's Trichrome (University of Melbourne Histology Platform), and scored by an experienced histopathologist in a blinded manner in accordance with the Clinical Research Network NAFLD activity score (NAS) [21] and Kleiner classification of liver fibrosis [65].

Triglyceride content

Whole liver was homogenised in 2 mL of 2:1 (v:v) chloroform-methanol. Subsequently, 600 µl of 0.9% NaCl was added, samples were vortexed, and spun at 2000 x g for 10 minutes. The bottom layer containing lipids was transferred to a new tube, gently dried under nitrogen gas, and reconstituted in 0.5 ml of 95% ethanol. Triglycerides were measured using a colorimetric assay (Triglycerides GPOPAP; Roche Diagnostics, Indianapolis, IN).

RNA extraction and PCR

RNA was isolated by homogenising liver samples in Trizol reagent (Sigma Aldrich, Cat# T9424). Samples were treated with DNAse (Ambion DNA free kit, ThermoFisher, VIC, Australia), reverse transcribed into cDNA using iSCRIPT reverse-transcriptase (Bio Rad, Cat# 1708890), and Real-time qPCR was performed using SYBR Green PCR master mix (Qiagen, Cat# 208056). Gene expression was determined using CFX Connect Real-time PCR and the delta-delta Ct method. Primer sequences are listed in Extended data **Table. 2**.

Precision cut liver slicing and EV secretion

Whole liver lobes from mice or a wedge biopsy from humans were placed in warm oxygenated M199 media (Thermo Fisher, Cat# 12340030) supplemented with 10% fetal bovine serum (Sigma Aldrich, Cat# F9423) and 1% penstrep. Liver lobes were mounted in 3% low-temperature gelling agarose (Lonza, Cat# 50110), and sectioned into 300 µM slices using a Krumdiek tissue slicer containing DMEM + 2% penstrep. Slices were then

washed in dPBS (Life Technologies, Cat# 14190250) and incubated in M199 + 1% penstrep at 37°C (95% O_2 + 5% CO_2) for 1 hour. Liver slices were then washed in dPBS and incubated for 16 hours in oxygenated EX-CELL protein-free media (Sigma Aldrich, Cat# 14340C) [9,23]. Conditioned medium was collected, and liver slices were weighed and snap frozen. To assess tissue viability, frozen whole liver and liver slices were pulverized, adenine nucleotides were extracted using 0.5 M PCA, and the ATP / ADP ratio was measured as per the manufacturer's instructions (Sigma Aldrich, Cat# MAK135). In separate studies, liver slices were treated with low (2 mM) or high (20 mM) glucose overnight and conditioned medium was collected for EV isolation. These experiments were repeated in the presence of high glucose, and presence or absence of insulin (10 nM), glucagon (20 pg/ml) or norepinephrine (15 pg/ml). For adipose EV secretion, epididymal white adipose tissue (~30 mg) were incubated in EX-CELL media for 6 hours. Conditioned media was collected for EV isolation.

EV isolation

Conditioned medium or serum was centrifuged at 3000 x g for 10 minutes and then at 10 000 x g for 30 minutes to remove large debris. Supernatents were filtered through a 0.2 µm PVDF filter, and small extracellular vesicles were pelleted at 100 000 x g for 1.5 hours. The supernatant was removed, and pellets were washed in dPBS and re-spun at 100 000 x g for 1.5 hours [66]. Final pellets were reconstituted in dPBS (i.e., saline), protein concentration was measured using a Pierce BCA assay (Life Technologies, Cat# 23225), and samples were stored at -80°C.

Endotoxin assay

To verify the purity of the EV isolations, serum and EVs were assessed for endotoxin levels using a Pierce chromogenic endotoxin kit (Thermo Fisher, Cat# A39552) as per the manufacturer's instructions.

Proteinase K and EV sonication experiments

Liver EVs from Control or NAFL mice were isolated, reconstituted at 1 µg / µl, and treated with or without proteinase K (Thermo Scientific, Cat# EO0491; 100 µg / ml) to 'shave' the EV surface proteins [35]. EVs were then incubated for 1.5 hours at 37 °C. To stop proteolysis, 3 mM of PMSF was added to samples on ice for 5 minutes. Samples were then spun at 16,100 x g for 1 hour at 4 °C to re-pellet the EVs, and protein concentration was re-assessed using a Pierce BCA assay. For sonication experiments, liver EVs were homogenised using a Q sonica sonicator at 30 amplitude for 30 seconds.

Immunoblotting

Isolated EVs and liver slices were reconstituted in RIPA buffer (65 mM Tris, 150 mM NaCL, 1% NP40, 0.5% sodium deoxycholate, 0.1% SDS, and 10% glycerol), protein was determined using a Pierce BCA assay, and samples were prepared for western blotting using 6X Lamelli buffer. Equal amounts of protein were loaded onto acrylamide gels for the Western blot detection of CD81 (1:1000, Abcam, Cat# ab109201), CD63 (1:1000, Abcam, Cat# ab134045), TSG101 (1:1000, Abcam, Cat# ab125011), CD9 (1:1000, Abcam, Cat# ab263019), HSP70 (1:1000, Abcam, Cat# ab181606), GLUT4 (1:1000, Abcam, Cat# ab33780), CAV3 (1:1000, Abcam, Cat# ab2912) and calnexin (1:1000, Abcam, Cat# ab22595). Proteins were separated using SDS-PAGE and transferred onto polyvinylidene difluoride membrane. Membranes were blocked with 5% non-fat milk and incubated with their appropriate primary and secondary antibodies (anti-rabbit, 1:2000, Cytiva, Cat# NA934V). Membranes were treated with chemiluminescence solution (Bio Rad, Cat# 1705060) and detected using enhanced chemiluminescence (Bio Rad).

Cryo-electron microscopy

Cryo-electron microscopy was used to assess the size and morphology of liver EVs (Bio21 institute Ian Holmes Imaging Centre, University of Melbourne). Liver EVs were added to a glow-discharged lacey carbon grid, vitrified and mounted into a cryo-holder (Gatan, Pleasanton, CA). Images were acquired using a 200 kV Tecnai G2 F30 System (FEI, The Netherlands). Size distribution of EVs were calculated from a minimum of 15 fields of view per sample [67].

Nano-particle tracking analysis

EV size and distribution was assessed using a ZetaView PMX-120 analyser and ZetaView Analyzer software (version 8.05.12). The system was calibrated as per manufacturers instructions with 100 nm Nanospheres 3100A. Analysis was performed in scatter mode at 25 °C. Each sample was diluted in dPBS to a final volume of 1 ml. Data was captured at a sensitivity of 80, shutterspeed 100, and frame rate 30. Post-acquisition settings were set to a minimum trace length of 10, minimum brightness 30, minimum area 5, and max area 1000 [68].

Imaging Flow Cytometry

Male C57BL/6J mice with healthy liver (12-15 weeks old, JAX 000664) or NAFL (~30 weeks old following dietary intervention) were fasted for 3 hours followed by gavage of water or glucose (2 g/kg). Blood was collected 10 minutes post-gavage and EVs were isolated as described above. Following EV isolation, fluorescent labelling was performed [69]. Isolated serum EV were incubated in 20 µl of filtered 0.2% BSA in PBS (BSA-PBS solution) containing 0.5 µg CD63-PE-Cy7 (Thermo Fisher, Cat# 25-06-31-82), 0.5 µg CD9-APC (Bio Legend, Cat# 124812), and 2.5 µl ASGPR1-PE (BD Biosciences, Cat# 563655) or PE Mouse IgG1 Kappa isotype control (BD Biosciences, Cat# 551436) for 1 hour in the dark at room temperature. EVs were diluted to 1 ml and spun at 100,000 x g for 1 hour. Pellets were reconstituted in BSA-PBS solution. Fluorescence signals were acquired on an AMNIS Imagestream X MkII Imaging Flow Cytometer (AMNIS/Millipore) using 60x objective at a low flow rate with the sample acquisition cut-off set to 5,000 events. Laser powers were adjusted to 150 mW for both 561 nm and 642 nm lasers. Brightfield signals were acquired in channel 1 (Ch01) and 9 (Ch09), side scatter in channel 12 (Ch12), PE in channel 3 (Ch03), PE-Cy7 in channel 6 (Ch06), and APC in channel 11 (Ch11). Data analysis was performed using IDEAS software. First, all events were gated based on the brightfield signals using the Gradient RMS feature to remove any acquired signals that were not in focus. Then, aspect ratio was plotted against area of acquired particles to discriminate EV and speed beads (previously optimised). Particles with an area smaller than the speed beads were gated. Fluorescence signals from Ch06 were then plotted against Ch11 to identify the double positive population. The Ch03 signals were plotted on a histogram and gated based on the isotype control.

Proteomics

Protein disulphide bonds for EV proteins (10 µg) were reduced at 65°C with 10 mmol/L (Tris(2-carboxyethyl)phosphine) for 20 minutes. Samples were mixed with 6.6 x volume of 8 M urea, added to a Microcon-30 kDa Centrifugal Filter (Sigma-Aldrich), and centrifuged at 14,000 × g (15 min) at 14 °C. Subsequently, 200 µl of 8 M Urea was added and samples were re-spun. Proteins were alkylated with 100 mM chloroacetamide (10 µL) and 8 M urea (90 µL) for 20 minutes at room temperature, centrifuged at 14,000 x g, washed and re-spun twice with 8 M urea, and washed 3x with 50 mM ammonia bicarbonate (pH=8.5). Proteins were digested with trypsin (1 µg trypsin / 100 µg of protein, 50 mM ammonia bicarbonate) overnight at 37 °C. Peptides were washed twice by adding 50 mM of ammonia bicarbonate (40 µL) to the Centrifugal Filter, and spun at 14,000 x g (15 min). Peptides were eluted in 0.5 M NaCl (50 µL), acidified to pH=3.0 with formic acid, purified with Millipore® C18 Ziptips (Agilent, Cat# A57003100), and dried using a Speedvac (Eppendorf Concentrator Plus, Germany). Purified peptides were reconstituted in 0.1% formic acid, centrifuged at 16,000 x g, and transferred to liquid chromatography vials for

analysis through liquid chromatography tandem mass spectrometry (Nano-ESI-LC-MS/MS) using an Orbitrap Elite mass spectrometer [9]. Data was analysed using MaxQuant (version 1.4.10.0 or 2.4.10.0) and Perseus software (version 1.6.0.7). Bioinformatics for pathways enrichment analysis was performed using Metascape [70] and Ingenuity Pathways Analysis (Qiagen).

Phosphoproteomics

Muscles were lysed in 2% SDS in 100 mM Tris, pH 8.5 and quantified by BCA (Thermo Scientific). Six hundred micrograms of protein was reduced with 10 mM Tris(2-carboxyethyl)phosphine hydrochloride and 40 mM 2-choroacetamide at 45°C for 5 minutes. Proteins were purified using single-pot, solid-phase-enhanced sample SP3 beads [71]. Briefly, proteins were bound to a 1:1 mix of 400mg hydrophilic:hydrophobic beads (GE; #45152105050250 and #65152105050250) at room temperature in 50% ethanol. The beads were washed three times with 80% ethanol, briefly dried at room temperature for 15 minutes and resuspended in 100 µL of 10% trifluroethanol in 100mM HEPEs pH 7.4. Protein was digested on the beads with 12 µg of sequencing grade trypsin (Sigma Aldrich) and sequencing grade LysC (Wako, Japan) overnight at 37°C while shaking at 1,800 RPM. Peptide supernatant was collected and transferred to a LoBind deep-96-well plate (Eppendorff) and the beads washed with 190 µL of water at 37°C while shaking at 1,800 RPM for 5 minutes. The peptide supernatant was removed and pooled with the peptides in the 96-well plate. Phosphopeptides were enriched with EasyPhos [72]. Briefly, Peptides were incubated with 7.2 mg of TiO_2 beads (GL Sciences, #5010-21315) in 50% isopropanol containing 1 mM KH_2PO_4 and 5% trifluoroacetic acid (TFA) for 5 minutes at 40°C while shaking at 1800 RPM. Beads were washed five times with 60% isopropanol containing 6% TFA and phosphopeptides eluted with 5% ammonium hydroxide solution in 40% acetonitrile. Phosphopeptides were dried and resuspended in 99% isopropanol containing 1% TFA and desalted with SDB-RPS micro-columns [72].

Peptides were resuspended in 2% acetonitrile (2%) with 0.1% trifluoracetic acid and separated on a Dionex 3500 nanoHPLC over a linear gradient of 3–40% Buffer B for 90 min (80% v/v acetonitrile, 0.1% v/v FA) on a 50 cm × 75 µm column maintained at 50°C containing C18AQ (1.9 µm; Dr Maisch, Ammerbuch, Germany) (PepSep, Marslev, Denmark) at a constant flow rate (300 nL/min). The peptides were ionized via electrospray ionization in positive mode with 1.9 kV at 275 °C and RF set to 40% into an an Orbitrap Eclipse mass spectrometer (ThermoFischer Scientific). The instrument was operated in data-independent acquisition mode with an MS1 spectrum (mass range 360–1033 m/z; 60,000 resolution, 2.5 x 10^6 automatic gain control (AGC) and 50 ms maximum injection time) followed by HCD MS/MS analysis of 50 windows with 13.7 m/z isolation and 1 m/z

overlap between the windows (30% normalized collision energy, 30,000 resolution, 1 x 10^6 AGC, 55 ms injection time). Data were searched with Spectronaut 15.7.220308.50606 using default parameters against the UniProt mouse database (June 2021; UP000000589_109090 and UP000000589_109090_additional) and peptide spectral matches, peptide and protein false discovery rate (FDR) set to 1%. Peptides were searched with variable modifications methionine oxidation and phosphorylation of Serine, Threonine and Tyrosine while carbamidomethylation set as the fixed modification. MS2-based extracted ion chromatograms were used for quantification employing 3-6 fragment ions >450 m/z with automated fragment-ion interference removal [73]. Data were processed with Perseus [74] to remove decoy data and potential contaminants. The Perseus Plugin Peptide collapse v 1.4.3 was used to convert a normal Spectronaut report into a site-level report [75] (https://github.com/AlexHgO/Perseus_Plugin_Peptide_Collapse). Data were Log_2-transformed and normalized by to the median area of each sample. Data were filtered to contain phosphosites quantified in at least 3 biological replicates of a single group and statistical analysis performed with ANOVA and t-tests including correction for multiple hypothesis testing using Benjamini Hochberg FDR with $q<0.05$ defined as the significance cut-off.

Glucose-tolerance test (GTT) and insulin tolerance test (ITT)

Mice were fasted and injected intraperitoneally (i.p) or intravenously (i.v) with either saline, empty liposomes, or 30 µg EVs secreted from liver, adipose tissue, or serum 1 hour prior to all functional analyses. Mice were gavaged or injected intraperitoneally with glucose (2 g/kg body weight), and blood glucose was measured over time (0, 15, 30, 45, 60, 90, 120 minutes) using a glucometer. For ITTs, mice were intraperitoneally injected with 1U/kg insulin and blood glucose was monitored at 0, 15, 30, 45, 60, and 90 minutes.

Serum measurements

During the GTT, serum was collected for the measurement of insulin at 0, 15, and 30 minutes. Insulin was measured using an insulin ELISA as per the manufacturers instructions (Crystal Chem, Cat# 90080). In fasted mice, circulating serum aminoalaninetransferase (ALT) levels were assessed using spectrometry [23].

Calorimetry

Energy expenditure, physical activity, VO_2 / VCO_2, and respiratory exchange ratio were determined using indirect calorimetry via a 16 chamber Promethium system (Sable Systems International). Studies were initiated following

12 hour acclimatisation, and data were collected 2 hours after an acute injection of either saline or liver EVs during the light cycle. Carbohydrate and fat oxidation were calculated using the VO_2 and VCO_2 measurements provided by the Promethium using the following equations [76]:

Carbohydrate oxidation: 4.585 * VCO_2 (L/min) – 3.226 * VO_2 (L/min);

Fat oxidation: 1.695 * VO_2 (L/min) – 1.701 * VCO_2 (L/min).

Values were divided by 60 and multiplied by 16.19 (carbohydrate) and 40.80 (fat) to convert into kilojoules per hour [76,77].

Hepatocyte isolation and hepatic glucose output

Primary hepatocytes were isolated using collagenase perfusion [23]. The liver was perfused through the inferior vena cava with HBSS buffer containing 0.5 mM EGTA for 15 minutes then digested using 50 mg collagenase H (Roche, Cat# 11074032001) in HBSS buffer containing 2 mM $CaCl_2$. Hepatocytes were plated on collagen-coated 6 well plates (500,000 cells/well), and treated with adherence media (M199, 100 U penicillin/streptomycin, 0.1% BSA, 2% FBS, 100 nM dexamethasone) overnight. To assess glucose output, hepatocytes were serum starved for 3 hours and then treated with glucose-free DMEM (Thermo Fisher, Cat# A1443001) for 30 minutes. Hepatocytes were then primed with or without insulin (100 nM) for 10 minutes, and then provided fresh phenol-red free glucose-free medium containing pyruvate (2 mM) and lactate (1 mM) in the absence or presence of insulin for 1 hour. Glucose output was assessed in the conditioned medium using a glucose oxidase assay (Thermo Fisher, Cat# CDT15221).

Islet isolation and insulin secretion

Mice were euthanised by cervical dislocation. The ampulla of vater was clamped using adhesion forceps, and 3 ml of HBSS (Sigma Aldrich, Cat# H6648) containing 0.35 mg / ml collagenase P (Sigma Aldrich, Cat# 11213857001) was slowly injected into the bile duct proximal to the liver. The inflated pancreas was extracted, and islets were isolated and counted [78]. Islets were allocated to 10-15 per condition, and treated with or without liver EVs (10 mg/ml) for 1 hour. Glucose-stimulated insulin secretion was performed under basal (2.8 mM) or high (20 mM) glucose for 1 hour in the presence of various secretagogues/inhibitors that include: 275 µM tolbutamide (Sigma Aldrich, Cat# T0891), 200 µM diazoxide (Sigma Aldrich, Cat# D9035), 10 nM Exendin-4 (Sigma Aldrich, Cat# HY-13443), 20 mM arginine, and 10 mM alanine. The supernatant and islets were collected for the measurement of insulin using an Insulin ELISA (Crystal Chem).

686

687 *Islet glucose oxidation and measurement of ATP / ADP ratio*

688 Isolated islets from mice were pre-treated in KREBS containing 2.8 mM glucose in the presence of saline or liver
689 EVs for 1 hr. For glucose oxidation, islets were treated in low (2.8 mM) or high (20 mM) glucose DMEM in the
690 presence of 14C glucose (Perkin Elmer, Cat# NEC852050UC) and saline or liver EVs for 3 hours. Conditioned
691 medium was collected and treated with 1 M perchloric acid. CO_2 was harvested in 300 µl of 1M sodium hydroxide
692 and transferred into scintillation fluid for counting (TRICARB, Perkin Elmer). For ATP / ADP ratio experiments,
693 islets were stimulated for 1 hour in KREBS buffer containing 2.8 mM or 20 mM glucose in the presence of saline
694 or liver EVs. Adenine nucleotides were extracted from islets with 0.5 M perchloric acid and neutralised with 2.3M
695 $KHCO_3$ (acid:base =3:1). Relative concentrations of ATP and ADP were measured using LC-MS on a QTRAP®
696 5500 mass spectrometer (AB-SCIEX).

697

698 *2-Deoxy-glucose uptake*

699 Soleus muscle, epididymal adipose tissue (~30mg), or brown adipose tissue (~20mg) were incubated in KREBS
700 (4.5% NaCl, 5.75% KCl, 6.1% $CaCl_2$, 10.55% KH_2PO_4, 19.1% $MgSO_4$ $7H_2O$, 1.3% $NaHCO_3$, 8 mM mannitol, 0.5%
701 BSA) containing 2 mM pyruvate for 30 minutes and shaking at 30°C. For insulin-stimulated glucose uptake, tissues
702 were then incubated in KREBS buffer supplemented with cold 10 µM 2-deoxy-glucose (2-DG) in the presence or
703 absence of 10 nM insulin for 20 minutes. Media was replaced with fresh KREBS buffer containing 10 µM cold 2-
704 DG, ^{14}C mannitol (Perkin Elmer, Cat# NEC852050UC), and ^{3}H 2-DG (Perkin Elmer, Cat# NET328A001MC) in the
705 presence or absence of 10 nM insulin for 10 minutes. For glucose effectiveness experiments, C2C12 (ATCC,
706 CRL_1772) cells or soleus muscle were treated with 2 µM, 10 µM, or 20 µM cold 2-DG in the presence of ^{3}H 2-
707 DG (Perkin Elmer, 0.5 µCi/ml) and ^{14}C mannitol (Perkin Elmer, soleus only; 0.2 µCi/ml) for 10 minutes. Samples
708 were treated in the presence of saline or liver EVs throughout the incubation steps, with or without the SR calcium
709 release inhibitor dantrolene (5 µM) or CaMKII inhibitor KN-62 (10 µM). Tissues/cells were rinsed twice in dPBS,
710 homogenized in dPBS, added to scintillation fluid, and counted for glucose uptake (TRICARB, Perkin Elmer).

711

712 *Hyperinsulinemic euglycemic clamp*

713 Mice were anesthetised and a catheter was inserted into the jugular vein. Following 3 days of recovery, mice were
714 fasted for 3 hours prior to beginning the clamp under conscious unrestrained conditions. Hyperinsulinemic-
715 euglycemic clamps were performed with continuous infusion of insulin (4 mU / kg / min) and exogenous glucose

(25% w/v) was infused to maintain blood glucose levels at ~ 8 mmol/L. Tail bloods were collected at 10 minute intervals for ~120 minutes as used previously by our lab [79].

Lateral ventricle cannulations

Under anesthesia by isofluorane, mice were implanted stereotaxically with guide cannulas into the lateral ventricle (0.2 mm posterior, 0.1 mm lateral from bregma) [80]. The tip of the guide cannula was positioned 1 mm above the injection site (1 mm ventral to the surface of the skull). Mice were allowed to recover for 4-5 days post-cannulation. Mice were administered an intracerebral ventricular injection of saline or liver EVs (16 µg) in a volume of 2 µl per animal 3 hours and 1 hour prior to a glucose tolerance test (2 mg / kg) as described above.

Plasma membrane and intracellular microsome fractionation

STZ treated mice were fasted, matched for basal glucose levels, and injected with either saline or liver EVs (30 µg). 1 h later, mice were gavaged with water (vehicle) or glucose (2 g/kg) and culled 30 min after. The gastrocnemius muscles were rapidly dissected and snap frozen. Frozen muscle was powdered and the plasma membrane and intracellular microsomes were fractionated [81-83]. Powdered muscle was homogenised in buffer A (250 mM sucrose, 10 mM Tris, 0.5 mM EDTA, pH 7.4) using a glass homogeniser and centrifuged at 16,000 x g for 20 min at 4°C. The supernatant was collected and spun at 43,000 x g for 30 min. The pellet was collected in RIPA buffer and reflects the microsomal fraction. The initial pellet was reconstituted in Buffer A, layered on top of Buffer B (1.12 M sucrose, 10 mM Tris, 0.5 mM EDTA, pH 7.4), and spun at 158,000 x g for 20 min. The interphase was collected, diluted in buffer A, and spun at 48,000 x g for 30 min to pellet the plasma membrane fraction.

Statistics

Animal studies and cell culture data are expressed as mean ± SEM. Patient characteristics are presented as mean ± SD. No statistical methods were used to pre-determine sample sizes but our sample sizes at minimum are similar to those reported in previous publications [9,17,23]. Individual data points were removed from analyses if they were identified as a statistical outlier using Grubbs' test, or if there was a clear technical experimental error. With the exception of NAS scoring of mouse and human liver, data collection and analysis were not performed blind to the conditions of the experiments. Data was analysed using Microsoft Excel, SigmaPlot version 11 or Graphpad Prism version 9.0.1. Normality was tested using a Shapiro-Wilk test. Statistical analysis was determined using unpaired or paired t-tests, one-way ANOVA, two-way ANOVA, or two-way repeated measures ANOVA followed by a

Student Newman Keuls post-hoc test, or Kruskall Wallis ANOVA on ranks followed by a Dunn's test, where appropriate. A P value of <0.05 was considered statistically significant.

DATA AVAILABILITY

All data is available within the manuscript, extended data, source data files, and supplemental files. The analysis in this study has used standard techniques and protocols without generating new unique reagents or custom code. The proteomic and phosphoproteomic data generated in this study are deposited to the ProteomeXchange Consortium (http://proteomecentral.proteomexchange.org/cgi/GetDataset) via the PRIDE [84], under the identifiers PXD037924, PXD036400, and PXD043137. These data are also provided as supplemental information.

ACKNOWLEDGEMENTS

We thank the team at the Ian Holmes Imaging Centre and Melbourne Mass Spectrometry and Proteomics facility of the Bio21 Institute at the University of Melbourne for instrument support, the infrastructure within the Melbourne Murine Metabolic Phenotyping Platform (MMMPP) for calorimetry assessment, the Melbourne Histology Platform at the University of Melbourne, Mitch Shambrook (La Trobe University) for instrument support for the NTA, Darryl Johnson for technical assistance with running Imaging Flow Cytometry, and Damien Keating (Flinders University) and Melkam Kebede (University of Sydney) for helpful discussions. **P.M.M** was supported by post-doctoral fellowships through the Natural Sciences and Engineering Research Council of Canada (NSERC, PDF-516731-2018) and Canadian Institutes of Health Research (CIHR, application # 430145). This work was supported by an NHMRC Ideas grant (**M.J.W**, **P.M.M**, **P.R.B**, APP1184309), NHMRC Investigator grants (**P.M.M**, APP2018187; **B.J.P**, APP2009642**),** a Diabetes Australia Research Trust grant (**P.M.M**), an MDHS Early Career Researcher grant (**P.M.M**, ECR1782020) and Department of Anatomy and Physiology seed grant (**P.M.M**). Graphical illustrations were created with BioRender.com.

AUTHOR CONTRIBUTIONS

P.M.M and **M.J.W** conceptualised the study design and funded the research. **P.M.M, C.H.Y, S.N.K, W.D.N, C.B, G.F, G.T.D** and **B.L.P** performed experiments. **P.M.M, C.H.Y, S.N.K, G.F, and B.L.P** analysed data. **G.T.D, A.F.H, B.L.P,** and **K.L** provided resources and guided experimental design. **P.R.B** provided human samples**.** **P.M.M**. and **M.J.W** wrote the manuscript. All authors edited the manuscript.

DECLARATION OF INTERESTS

MJW has received research funding from Gilead Sciences and CSL, and honoraria from Gilead Sciences. The remaining authors declare no competing interests.

FIGURE LEGENDS

Fig. 1. Confirmation of NAFL and NASH and validation of small extracellular vesicle isolation secreted from livers of mice

(A) Representative micrographs of H&E and Masson's trichrome stained liver sections obtained from mice fed a control (n=8), NAFL (n=10), or NASH (n=10) diet in 1 cohort. Scale bar = 100 μm.

(B) Liver triacylglycerol accumulation in response to dietary interventions (n=5 control, n=6 NAFL, n=6 NASH). *, significant from Control in 1 experiment. P=0.007.

(C) NAFL activity score (NAS) grading based on histological assessment of steatosis, hepatocyte ballooning, and inflammation (n=8 control, n=10 NAFL, n=10 NASH) in 1 cohort. *, significant from Control; #, significant from NAFL. P<0.001.

(D) Serum alanine aminotransferase (ALT) levels (n=22 control, n=12 NAFL, n=10 NASH) in 1 experiment. *, significant from Control. P<0.001.

(E) Liver mRNA expression of inflammation and fibrosis markers across 3 experiments. *, significantly different from Control; #, significant from NAFL. P<0.05. Detailed n-sizes and P-values for each marker provided in Source data.

(F-G) Representative nanoparticle tracking analysis (F, n=12 biological replicates, average presented) and cryo-electron microscopy (G, n=1) of liver EVs. Scale bar = 100 nm.

(H) Representative immunoblot showing the presence of common exosome markers in liver slices (n=2) and EVs (n=2) and the absence of calnexin, a marker of the endoplasmic reticulum across 1 experiment. The representative stain-free blot is from the HSP70 blot.

(I-K) EV secretion from murine liver slices. (I) Total particles secreted from whole liver (n=8 control, n=11 NAFL, n=5 NASH, P=0.009). (J) Liver EV protein secretion relative to liver slice mass (n=22 control, n=14 NAFL, n=15 NASH, P<0.001). (K) Total EV protein secretion per liver (n=29 control, n=14 NAFL, n=14 NASH, P=0.236) from 1 experiment. *, significant from Control; #, significant from NAFL.

Data are expressed as mean ± SEM. Each datapoint represents an independent biological sample. Data was analysed using a one-way ANOVA with Student-Newman-Keuls post-hoc analysis (C, D, E, I, J, K) or Kruskall-Wallace one-way ANOVA on ranks with Dunn's comparison (B, E).

Fig. 2. The liver EV proteome in mice with NAFL and NASH

(A) Venn diagram showing the number of proteins common and unique to liver EVs secreted from control, NAFL, and NASH livers. n=10/group.

(B) Principal component analysis of proteomic group clustering of liver EV samples from control, NAFL, and NASH livers (n=10/group).

(C-E) Volcano plot comparison of the liver EV proteome in NAFL relative to healthy control mice (C), NASH relative to healthy control mice (D), and NASH relative to NAFL mice (E). n=10/group. Top 5 up- or down- differentially regulated proteins are presented for comparisons of NAFL and NASH relative to Control (inset). $q<0.05$.

(F-G) Selective pathways enrichment in NAFL relative to control (F), and NASH relative to control mice (G). n=10/group. *P* values indicated within figure.

Data was analysed using principle component analysis (B), or unpaired two-tailed t-test for individual comparisons relative to control mice (C, E). Data reflects independent biological samples.

Fig. 3. Liver-secreted EVs improve glycemic control

(A-C) Oral glucose tolerance test (GTT) in control mice (A, n=8 saline, n=9 NAFL EV, n=7 NASH EV), NAFL mice (B, n=8/group), or NASH mice (C, n=8 saline, n=9 Control EV) in response to intraperitoneal injection of saline/liver EV across 1 cohort per diet. *, significant from Control EV or NAFL EV, #, significant from NASH EV. $P<0.001$.

(D-F) Serum insulin during the GTT in control (D, n=5 saline, n=6 NAFL EV, n=5 NASH EV), NAFL (E, n=8 saline, n=7 Control EV), and NASH (F, n=9 saline, n=7 Control EV) mice in response to saline or liver EV administration across 1 experiment. *, significant from Saline. $P<0.05$.

(G-H) Nanoparticle tracking analysis (G, $P<0.001$) and protein content (H, $P=0.007$) of liver secreted EVs in response to low (2 mM) or high (20 mM) glucose across 2 experiments (n=7/group/measurement). *, significant from low glucose.

(I-K) Imaging flow cytometry of $ASGPR^+$ (liver EV marker) serum EVs ($CD63^+$ / $CD9^+$) derived from control (I, J, n=4/group, $P=0.03$) or NAFL (K, n=3 vehicle, n=4 glucose, $P=0.88$) mice in response to fasting (water vehicle) or glucose gavage across 1 experiment for each cohort. *, significant from Fasted.

(L-M) Blood glucose (L) and plasma insulin (M) during a GTT in control (n=6/group) and NAFL mice (n=5/group) in response to saline or sonicated liver EVs across 1 cohort per diet. $P<0.001$.

(N-Q) Blood glucose and plasma insulin during a GTT in control (N, n=8 saline, n=10 NAFL EV, n=10 'shaved' EV, $P<0.001$; O, n=9/group, $P<0.05$) and NAFL (P, n=5 saline, n=5 Control EV, n=6 'shaved' EV, $P<0.001$; Q, n=9

saline, n=9 Control EV, n=11 'shaved' EV, $P<0.05$) in response to saline or 'shaved' EVs across 2 experiments each condition. *, significant from Saline; #, significant from Shaved EV.

Data are expressed as mean ± SEM. Each datapoint represents an independent biological sample. Data was analysed using repeated measures two-way ANOVA (A, B, C, E, N, O, P), two-way ANOVA (D, F, G, Q), or three-way ANOVA (L, M) with Student-Newman-Keuls post-hoc, or two-tailed t-test (paired, H; unpaired, J, K).

Fig. 4. Liver-secreted EVs do not regulate insulin sensitivity

(A-B) Blood glucose levels following intraperitoneal insulin administration (1 IU / kg) in control (A, n=6 saline, n=7 NAFL EV) and NAFL (B, n=13 saline, n=9 Control EV) mice that received an intraperitoneal injection of saline or liver EVs across 1 experiment for each cohort. $P<0.001$ (main effect: Time).

(C) Glucose output from primary hepatocytes obtained from Control mice treated *ex vivo* with saline or liver EVs (10 µg/ml) for 1 hr prior to and during the experiment (n=5 saline/basal, n=6 saline/insulin, n=3 EV/basal, n=6 EV/insulin) across 1 experiment from 6 mice. *, significant main effect of insulin relative to basal. $P=0.002$.

(D-F) Glucose uptake in isolated soleus muscle (D, n=6/group, $P<0.001$, basal and insulin-stimulated samples are paired from the same animal within each treatment), white adipose tissue (E, n=4 saline, n=5 NAFL EV, $P=0.649$), and brown adipose tissue (F, n=4/group, $P=0.672$) obtained from Control mice treated *ex vivo* with saline or liver EVs (10 µg/ml) from NAFL mice 1 hr prior to and during the experiment. 1 experiment for each tissue. Basal and insulin-stimulated samples from adipose are paired from the same animal across saline and liver EV treatments.*, significant main effect of insulin relative to basal.

(G) Rate of glucose infusion during a hyperinsulinemic-euglycemic clamp in control mice that received an intraperitoneal injection of saline or liver EVs 1 hr prior to the clamp in 1 independent cohort (n=7/group). $P=0.63$.

Data are expressed as mean ± SEM. Each datapoint represents an independent biological sample. Data was analysed using a two-way ANOVA (A, C, D, E, F) or repeated measures two-way ANOVA (B) with Student-Newman-Keuls post-hoc, or unpaired two-tailed t-test (G).

Fig. 5. Liver EVs improve glycemic control through enhanced glucose effectiveness

(A-B) Blood glucose (A) and insulin (B) during an oral GTT in streptozotocin (STZ) treated mice in response to intraperitoneal injection of saline or liver EVs (n=4 control saline, n=6/group for STZ conditions) across 1 experiment. $P<0.001$ for blood glucose (STZ comparison only), $P=0.213$ for insulin (STZ comparison only), $P=0.01$

(15-min insulin time-point per group). *, significant from STZ + saline injection; #, significant from STZ + liver EV injection.

(C-D) Blood glucose during an intraperitoneal GTT in control (C, n=6/group) or NAFL (D, n=7 saline, n=6 Control EV) mice in response to saline or liver EVs across 1 cohort. $P<0.001$.

(E) Whole body carbohydrate oxidation in control mice over 2 hrs in response to saline or liver EVs (n=4/group) across 1 experiment. $P=0.026$). *, significant from Saline.

(F-G) Glucose-dependent glucose uptake in C2C12 myotubes (F, n=9 saline/2 μM and 10 μM, n=7 saline/20 μM, n=9/liver EV conditions, $P=0.208$ (2 μM), $P=0.794$ (10 μM), $P=0.03$ (20 μM, across 4 independent experiments and 6 EV donors) or mouse soleus (G, n=5 saline/2 μM, n=7 saline/20 μM, n=5 liver EV/2 μM, n=7 liver EV/ 20 μM, $P=0.04$, from 12 independent mice)) treated with saline or liver EVs. *, significant from saline within 20 μM; #, significant from 2 μM within same condition.

(H-I) Plasma membrane (H, n=8 saline/water, n=8 saline/HG, n=9 EV/HG, $P=0.012$) and microsomal (I, n=7 saline/water, n=7 saline/HG, n=9 EV/HG, $P<0.05$) GLUT4 in muscle from STZ mice in response to saline or liver EVs and gavage of water or saline/liver EV and glucose across 2 cohorts. *, significant from saline/vehicle; #, significant from saline/HG. HG, high glucose; Veh, vehicle.

Data are expressed as mean ± SEM. Data points represent independent biological samples. Data was analysed using a two-way ANOVA (G) or repeated measures two-way ANOVA (A, B, C, D) with a Student-Newman-Keuls post-hoc, a one-way ANOVA (B (15-min time-point), H, I) with a Student-Newman-Keuls, or unpaired two-tailed t-test (E, F).

Fig. 6. Liver EV's activate cell signalling associated with calcium metabolism

(A-B) Differentially regulated phosphosites between soleus muscles treated *ex vivo* with high glucose relative to low glucose (A, n=4 LG/saline, n=-5/HG or HG/EV groups) or high glucose + liver EVs (B, n=5 HG, n=5 HG/EV) relative to high glucose/saline across 1 experiment. $q<0.05$

(C-D) List of proteins downregulated (C) or upregulated (D) in response to high glucose in the absence or presence of liver EVs (proteins highlighted in black text represent common proteins identified across analyses) across 1 experiment. Created with BioRender.com. $q<0.05$.

(E-H) Glucose-dependent glucose-uptake in soleus (E, F) or C2C12 (G, H) treated with dantrolene (E, n=3 saline, n=5/ HG groups, $P<0.001$, 8 mice; G, n=9 saline, n=8/HG groups, $P<0.001$) or KN-62 (F, n=3 saline, n=8/HG

groups, *P*<0.001, 11 mice); H, n=8 saline, n=9/HG groups, *P*<0.001) in response to saline or NAFL EVs across 4 experiments. *, significant from low 2-deoxyglucose saline (2 μM, LG), #, significant from high 2-deoxyglucose saline (2 μM,in same group).

Data are expressed as mean ± SEM. Data points represent independent biological samples. Data was analysed using a two-way ANOVA (G) or repeated measures two-way ANOVA (A, B, C, D) with a Student-Newman-Keuls post-hoc, a one-way ANOVA (E, F) or Kruskal-Wallis one-way ANOVA on Ranks (G, H) with a Student-Newman-Keuls or Dunn's post-hoc, or unpaired two-tailed t-test (A, B).

Fig. 7. Liver-secreted EVs directly stimulate GSIS in primary murine islets

(A) Glucose-stimulated insulin secretion (GSIS) in primary islets treated 1 hr prior to and during the experiment with saline, NAFL liver EVs (10 μg/ml), or NAFL liver EVs treated with Proteinase K (10 μg/ml) to 'shave' EV surface proteins (n=5/ 2.8 mM groups, n=7 saline/20 mM, n=5 untreated EV/20 mM, n=4 shaved EV/20 mM). *P*=0.029 across 1 independent experiment. *, significant from low glucose within same condition (i.e., saline, untreated EV, or shaved EV); #, significant from saline + high glucose; †, significant from untreated EV + high glucose.

(B) Overview of islet insulin secretion and secretagogue / inhibitor involvement. Schematic was recreated and modified from a previous publication [45]. Created with BioRender.com.

(C-D) Glucose oxidation (C, n=8/group, *P*=0.04 isolated from 9 independent mice) and ATP/ADP ratio (D, n=9 Saline/2.8 mM, n=10 saline/20 mM, n=10 NAFL EV/2.8 mM, n=12 NAFL EV/20 mM, *P*<0.001 (main effect), isolated from 11 independent mice) in primary islets in the absence or presence of 10 μg/ml NAFL EVs across 3 experiments/measurement. *, significant from low glucose within the same condition (i.e., Saline or NAFL EVs).

(E-F) The ratio of GSIS in the presence of high / low glucose concentrations in response to tolbutamide (E, n=10 saline, n=11 NAFL EV, *P*=0.966) and Diazoxide (F, n=4 saline, n=6 NAFL EV, *P*=0.26).

(G-I) The ratio of GSIS in primary islets treated with Arginine (G, n=6/group, *P*=0.05), alanine (H, n=10 saline, n=11 NAFL EV, *P*=0.04), and Exendin 4, a GLP receptor agonist (I, n=5/group, *P*=0.364) across 2 experiments involving isolations from 9 mice. *, significantly different from Saline.

Data are expressed as mean ± SEM. Data was analysed using a two-way ANOVA (A, C, D, H) paired two-tailed t-test (G, I), or unpaired two-tailed t-test (E, F). *P*<0.05.

Fig. 8. Human liver-secreted EVs improve glycemic control

(A) Overview of the experimental design for human tissue collection, EV isolation and administration into mice. Created with BioRender.com.

(B) NTA of liver EVs obtained from humans with healthy liver or NAFL/NASH (n=7 healthy female, n=7 NAFL/NASH pooled - 5 female/2 male). *P*=0.73.

(C) Blood glucose levels during an oral glucose tolerance test (GTT) in NOD/SCID mice that received saline or liver EVs (30 µg) obtained from human liver 1 hr prior to oral glucose gavage (n=7 for Saline, n=3 for 'Healthy', n=4 for NAFL. Note: EVs from 2-3 human donors were used per n=1 injection into mice. 7 female donors for 'healthy' and 5 female and 2 male donors for 'NAFL' EVs). *, significant from Saline. *P*<0.001.

(D) Serum insulin in NOD/SCID mice during the oral GTT (n=7 for Saline, n=6 for healthy/NAFL EV consisting of n=2 for Healthy, n=4 NAFL). Note: EVs from 2-3 human donors were used per n=1 injection into mice. 7 female donors for 'healthy' and 5 female and 2 male donors for 'NAFL' EVs). *, Significantly different from Saline.

EVs, small extracellular vesicles; NAFL, non-alcoholic fatty liver; NASH, non-alcoholic steatohepatitis. Data are expressed as mean ± SEM. Data points represent independent biological samples. Data was analysed using a two-way ANOVA (C, D) or unpaired two-tailed t-test (B, calculated from AUC).

References

1 Chalasani, N. *et al.* The diagnosis and management of nonalcoholic fatty liver disease: Practice guidance from the American Association for the Study of Liver Diseases. *Hepatology* **67**, 328-357, doi:10.1002/hep.29367 (2018).

2 Angulo, P. *et al.* Liver Fibrosis, but No Other Histologic Features, Is Associated With Long-term Outcomes of Patients With Nonalcoholic Fatty Liver Disease. *Gastroenterology* **149**, 389-397 e310, doi:10.1053/j.gastro.2015.04.043 (2015).

3 Younossi, Z. M. *et al.* Global epidemiology of nonalcoholic fatty liver disease-Meta-analytic assessment of prevalence, incidence, and outcomes. *Hepatology* **64**, 73-84, doi:10.1002/hep.28431 (2016).

4 Ooi, G. J. *et al.* Effect of Body Mass Index, Metabolic Health and Adipose Tissue Inflammation on the Severity of Non-alcoholic Fatty Liver Disease in Bariatric Surgical Patients: a Prospective Study. *Obes Surg* **29**, 99-108, doi:10.1007/s11695-018-3479-2 (2019).

5 Younossi, Z. M. *et al.* The global epidemiology of NAFLD and NASH in patients with type 2 diabetes: A systematic review and meta-analysis. *J Hepatol* **71**, 793-801, doi:10.1016/j.jhep.2019.06.021 (2019).

6 Korenblat, K. M., Fabbrini, E., Mohammed, B. S. & Klein, S. Liver, muscle, and adipose tissue insulin action is directly related to intrahepatic triglyceride content in obese subjects. *Gastroenterology* **134**, 1369-1375, doi:10.1053/j.gastro.2008.01.075 (2008).

7 Hwang, J. H. *et al.* Increased intrahepatic triglyceride is associated with peripheral insulin resistance: in vivo MR imaging and spectroscopy studies. *Am J Physiol Endocrinol Metab* **293**, E1663-1669, doi:10.1152/ajpendo.00590.2006 (2007).

8 Meex, R. C. *et al.* Fetuin B Is a Secreted Hepatocyte Factor Linking Steatosis to Impaired Glucose Metabolism. *Cell Metab* **22**, 1078-1089, doi:10.1016/j.cmet.2015.09.023 (2015).

9 Montgomery, M. K. *et al.* Deep proteomic profiling unveils arylsulfatase A as a non-alcoholic steatohepatitis inducible hepatokine and regulator of glycemic control. *Nat Commun* **13**, 1259, doi:10.1038/s41467-022-28889-2 (2022).

10 Watt, M. J., Miotto, P. M., De Nardo, W. & Montgomery, M. K. The Liver as an Endocrine Organ-Linking NAFLD and Insulin Resistance. *Endocr Rev* **40**, 1367-1393, doi:10.1210/er.2019-00034 (2019).

11 Jensen-Cody, S. O. & Potthoff, M. J. Hepatokines and metabolism: Deciphering communication from the liver. *Mol Metab* **44**, 101138, doi:10.1016/j.molmet.2020.101138 (2021).

12 Misu, H. *et al.* A liver-derived secretory protein, selenoprotein P, causes insulin resistance. *Cell Metab* **12**, 483-495, doi:10.1016/j.cmet.2010.09.015 (2010).

13 Xu, J. *et al.* Fibroblast growth factor 21 reverses hepatic steatosis, increases energy expenditure, and improves insulin sensitivity in diet-induced obese mice. *Diabetes* **58**, 250-259, doi:10.2337/db08-0392 (2009).

14 Montgomery, M. K. *et al.* SMOC1 is a glucose-responsive hepatokine and therapeutic target for glycemic control. *Sci Transl Med* **12**, doi:10.1126/scitranslmed.aaz8048 (2020).

15 Michael, D. J., Cai, H., Xiong, W., Ouyang, J. & Chow, R. H. Mechanisms of peptide hormone secretion. *Trends Endocrinol Metab* **17**, 408-415, doi:10.1016/j.tem.2006.10.011 (2006).

16 Isaac, R., Reis, F. C. G., Ying, W. & Olefsky, J. M. Exosomes as mediators of intercellular crosstalk in metabolism. *Cell Metab* **33**, 1744-1762, doi:10.1016/j.cmet.2021.08.006 (2021).

17 Ji, Y. *et al.* Hepatocyte-derived exosomes from early onset obese mice promote insulin sensitivity through miR-3075. *Nat Metab* **3**, 1163-1174, doi:10.1038/s42255-021-00444-1 (2021).

18 Albanese, M. *et al.* MicroRNAs are minor constituents of extracellular vesicles that are rarely delivered to target cells. *PLoS Genet* **17**, e1009951, doi:10.1371/journal.pgen.1009951 (2021).

19 Crewe, C. *et al.* An Endothelial-to-Adipocyte Extracellular Vesicle Axis Governed by Metabolic State. *Cell* **175**, 695-708 e613, doi:10.1016/j.cell.2018.09.005 (2018).

20 Ying, W. *et al.* Adipose Tissue Macrophage-Derived Exosomal miRNAs Can Modulate In Vivo and In Vitro Insulin Sensitivity. *Cell* **171**, 372-384 e312, doi:10.1016/j.cell.2017.08.035 (2017).

21 Brunt, E. M. *et al.* Nonalcoholic fatty liver disease (NAFLD) activity score and the histopathologic diagnosis in NAFLD: distinct clinicopathologic meanings. *Hepatology* **53**, 810-820, doi:10.1002/hep.24127 (2011).

22 European Association for the Study of the, L., European Association for the Study of, D. & European Association for the Study of, O. EASL-EASD-EASO Clinical Practice Guidelines for the management of non-alcoholic fatty liver disease. *J Hepatol* **64**, 1388-1402, doi:10.1016/j.jhep.2015.11.004 (2016).

23 De Nardo, W. *et al.* Proteomic analysis reveals exercise training induced remodelling of hepatokine secretion and uncovers syndecan-4 as a regulator of hepatic lipid metabolism. *Mol Metab* **60**, 101491, doi:10.1016/j.molmet.2022.101491 (2022).

24 Giebel, B. & Helmbrecht, C. Methods to Analyze EVs. *Methods Mol Biol* **1545**, 1-20, doi:10.1007/978-1-4939-6728-5_1 (2017).

25 Rontogianni, S. *et al.* Proteomic profiling of extracellular vesicles allows for human breast cancer subtyping. *Commun Biol* **2**, 325, doi:10.1038/s42003-019-0570-8 (2019).
26 Gidlof, O. *et al.* Proteomic profiling of extracellular vesicles reveals additional diagnostic biomarkers for myocardial infarction compared to plasma alone. *Sci Rep* **9**, 8991, doi:10.1038/s41598-019-45473-9 (2019).
27 Wang, S., Kojima, K., Mobley, J. A. & West, A. B. Proteomic analysis of urinary extracellular vesicles reveal biomarkers for neurologic disease. *EBioMedicine* **45**, 351-361, doi:10.1016/j.ebiom.2019.06.021 (2019).
28 Thompson, A. G. *et al.* CSF extracellular vesicle proteomics demonstrates altered protein homeostasis in amyotrophic lateral sclerosis. *Clin Proteomics* **17**, 31, doi:10.1186/s12014-020-09294-7 (2020).
29 Xie, Y. *et al.* Membrane-bound HSP70-engineered myeloma cell-derived exosomes stimulate more efficient CD8(+) CTL- and NK-mediated antitumour immunity than exosomes released from heat-shocked tumour cells expressing cytoplasmic HSP70. *J Cell Mol Med* **14**, 2655-2666, doi:10.1111/j.1582-4934.2009.00851.x (2010).
30 Deng, Z. B. *et al.* Adipose tissue exosome-like vesicles mediate activation of macrophage-induced insulin resistance. *Diabetes* **58**, 2498-2505, doi:10.2337/db09-0216 (2009).
31 Kim, D. K. *et al.* Chromatographically isolated CD63+CD81+ extracellular vesicles from mesenchymal stromal cells rescue cognitive impairments after TBI. *Proc Natl Acad Sci U S A* **113**, 170-175, doi:10.1073/pnas.1522297113 (2016).
32 Ding, M. *et al.* Exosomes Isolated From Human Umbilical Cord Mesenchymal Stem Cells Alleviate Neuroinflammation and Reduce Amyloid-Beta Deposition by Modulating Microglial Activation in Alzheimer's Disease. *Neurochem Res* **43**, 2165-2177, doi:10.1007/s11064-018-2641-5 (2018).
33 Peters, D. T. *et al.* Asialoglycoprotein receptor 1 is a specific cell-surface marker for isolating hepatocytes derived from human pluripotent stem cells. *Development* **143**, 1475-1481, doi:10.1242/dev.132209 (2016).
34 Kalluri, R. & LeBleu, V. S. The biology, function, and biomedical applications of exosomes. *Science* **367**, doi:10.1126/science.aau6977 (2020).
35 Charoenviriyakul, C., Takahashi, Y., Morishita, M., Nishikawa, M. & Takakura, Y. Role of Extracellular Vesicle Surface Proteins in the Pharmacokinetics of Extracellular Vesicles. *Mol Pharm* **15**, 1073-1080, doi:10.1021/acs.molpharmaceut.7b00950 (2018).
36 Roh, E., Song, D. K. & Kim, M. S. Emerging role of the brain in the homeostatic regulation of energy and glucose metabolism. *Exp Mol Med* **48**, e216, doi:10.1038/emm.2016.4 (2016).
37 Hu, X. *et al.* Extracellular vesicles from adipose-derived stem cells promote microglia M2 polarization and neurological recovery in a mouse model of transient middle cerebral artery occlusion. *Stem Cell Res Ther* **13**, 21, doi:10.1186/s13287-021-02668-0 (2022).
38 Alford, F. P., Henriksen, J. E., Rantzau, C. & Beck-Nielsen, H. Glucose effectiveness is a critical pathogenic factor leading to glucose intolerance and type 2 diabetes: An ignored hypothesis. *Diabetes Metab Res Rev* **34**, e2989, doi:10.1002/dmrr.2989 (2018).
39 Small, L. *et al.* Comparative analysis of oral and intraperitoneal glucose tolerance tests in mice. *Mol Metab* **57**, 101440, doi:10.1016/j.molmet.2022.101440 (2022).
40 Khatua, A. K., Taylor, H. E., Hildreth, J. E. & Popik, W. Exosomes packaging APOBEC3G confer human immunodeficiency virus resistance to recipient cells. *J Virol* **83**, 512-521, doi:10.1128/JVI.01658-08 (2009).
41 Xie, Z. *et al.* Adipose-Derived Exosomes Exert Proatherogenic Effects by Regulating Macrophage Foam Cell Formation and Polarization. *J Am Heart Assoc* **7**, doi:10.1161/JAHA.117.007442 (2018).
42 Gao, K. *et al.* Exosomes Derived From Septic Mouse Serum Modulate Immune Responses via Exosome-Associated Cytokines. *Front Immunol* **10**, 1560, doi:10.3389/fimmu.2019.01560 (2019).
43 Wilson-Grady, J. T., Haas, W. & Gygi, S. P. Quantitative comparison of the fasted and re-fed mouse liver phosphoproteomes using lower pH reductive dimethylation. *Methods* **61**, 277-286, doi:10.1016/j.ymeth.2013.03.031 (2013).
44 Linn, T. C., Pettit, F. H. & Reed, L. J. Alpha-keto acid dehydrogenase complexes. X. Regulation of the activity of the pyruvate dehydrogenase complex from beef kidney mitochondria by phosphorylation and dephosphorylation. *Proc Natl Acad Sci U S A* **62**, 234-241, doi:10.1073/pnas.62.1.234 (1969).
45 Campbell, J. E. & Newgard, C. B. Mechanisms controlling pancreatic islet cell function in insulin secretion. *Nat Rev Mol Cell Biol* **22**, 142-158, doi:10.1038/s41580-020-00317-7 (2021).
46 Pearson, T., Greiner, D. L. & Shultz, L. D. Humanized SCID mouse models for biomedical research. *Curr Top Microbiol Immunol* **324**, 25-51, doi:10.1007/978-3-540-75647-7_2 (2008).
47 Lo, J. C. *et al.* Obesity does not promote tumorigenesis of localized patient-derived prostate cancer xenografts. *Oncotarget* **7**, 47650-47662, doi:10.18632/oncotarget.10258 (2016).

48 Thomou, T. *et al.* Adipose-derived circulating miRNAs regulate gene expression in other tissues. *Nature* **542**, 450-455, doi:10.1038/nature21365 (2017).

49 Koenen, M. T. *et al.* Extracellular Vesicles from Steatotic Hepatocytes Provoke Pro-Fibrotic Responses in Cultured Stellate Cells. *Biomolecules* **12**, doi:10.3390/biom12050698 (2022).

50 Nemeth, K. *et al.* Extracellular vesicle release and uptake by the liver under normo- and hyperlipidemia. *Cell Mol Life Sci* **78**, 7589-7604, doi:10.1007/s00018-021-03969-6 (2021).

51 Yan, C. *et al.* A High-Fat Diet Attenuates AMPK alpha1 in Adipocytes to Induce Exosome Shedding and Nonalcoholic Fatty Liver Development In Vivo. *Diabetes* **70**, 577-588, doi:10.2337/db20-0146 (2021).

52 Zhang, R. *et al.* A Potential Target for Diabetic Vascular Damage: High Glucose-Induced Monocyte Extracellular Vesicles Impair Endothelial Cells by Delivering miR-142-5p. *Front Bioeng Biotechnol* **10**, 913791, doi:10.3389/fbioe.2022.913791 (2022).

53 Burger, D. *et al.* High glucose increases the formation and pro-oxidative activity of endothelial microparticles. *Diabetologia* **60**, 1791-1800, doi:10.1007/s00125-017-4331-2 (2017).

54 Povero, D. *et al.* Lipid-induced toxicity stimulates hepatocytes to release angiogenic microparticles that require Vanin-1 for uptake by endothelial cells. *Sci Signal* **6**, ra88, doi:10.1126/scisignal.2004512 (2013).

55 Sabatier, F. *et al.* Type 1 and type 2 diabetic patients display different patterns of cellular microparticles. *Diabetes* **51**, 2840-2845, doi:10.2337/diabetes.51.9.2840 (2002).

56 Tramontano, A. F. *et al.* Circulating endothelial microparticles in diabetes mellitus. *Mediators Inflamm* **2010**, 250476, doi:10.1155/2010/250476 (2010).

57 Cheng, V., Kashyap, S. R., Schauer, P. R., Kirwan, J. P. & McCrae, K. R. Restoration of glycemic control in patients with type 2 diabetes mellitus after bariatric surgery is associated with reduction in microparticles. *Surg Obes Relat Dis* **9**, 207-212, doi:10.1016/j.soard.2011.09.026 (2013).

58 Gesmundo, I. *et al.* Adipocyte-derived extracellular vesicles regulate survival and function of pancreatic beta cells. *JCI Insight* **6**, doi:10.1172/jci.insight.141962 (2021).

59 Mleczko, J. *et al.* Extracellular Vesicles from Hypoxic Adipocytes and Obese Subjects Reduce Insulin-Stimulated Glucose Uptake. *Mol Nutr Food Res* **62**, doi:10.1002/mnfr.201700917 (2018).

60 Pan, Y. *et al.* Adipocyte-secreted exosomal microRNA-34a inhibits M2 macrophage polarization to promote obesity-induced adipose inflammation. *J Clin Invest* **129**, 834-849, doi:10.1172/JCI123069 (2019).

61 Merrins, M. J., Corkey, B. E., Kibbey, R. G. & Prentki, M. Metabolic cycles and signals for insulin secretion. *Cell Metab* **34**, 947-968, doi:10.1016/j.cmet.2022.06.003 (2022).

62 Lopez-Bermudo, L. *et al.* Contribution of Liver and Pancreatic Islet Crosstalk to beta-Cell Function/Dysfunction in the Presence of Fatty Liver. *Front Endocrinol (Lausanne)* **13**, 892672, doi:10.3389/fendo.2022.892672 (2022).

63 Zhao, Y. *et al.* Liver governs adipose remodelling via extracellular vesicles in response to lipid overload. *Nat Commun* **11**, 719, doi:10.1038/s41467-020-14450-6 (2020).

64 Furman, B. L. Streptozotocin-Induced Diabetic Models in Mice and Rats. *Curr Protoc* **1**, e78, doi:10.1002/cpz1.78 (2021).

65 Kleiner, D. E. *et al.* Design and validation of a histological scoring system for nonalcoholic fatty liver disease. *Hepatology* **41**, 1313-1321, doi:10.1002/hep.20701 (2005).

66 Vella, L. J. *et al.* A rigorous method to enrich for exosomes from brain tissue. *J Extracell Vesicles* **6**, 1348885, doi:10.1080/20013078.2017.1348885 (2017).

67 Ma, C. *et al.* Extracellular Vesicles Secreted by Glioma Stem Cells Are Involved in Radiation Resistance and Glioma Progression. *Int J Mol Sci* **23**, doi:10.3390/ijms23052770 (2022).

68 Espejo, C. *et al.* Cathelicidin-3 Associated With Serum Extracellular Vesicles Enables Early Diagnosis of a Transmissible Cancer. *Front Immunol* **13**, 858423, doi:10.3389/fimmu.2022.858423 (2022).

69 van der Vlist, E. J., Nolte-'t Hoen, E. N., Stoorvogel, W., Arkesteijn, G. J. & Wauben, M. H. Fluorescent labeling of nano-sized vesicles released by cells and subsequent quantitative and qualitative analysis by high-resolution flow cytometry. *Nat Protoc* **7**, 1311-1326, doi:10.1038/nprot.2012.065 (2012).

70 Zhou, Y. *et al.* Metascape provides a biologist-oriented resource for the analysis of systems-level datasets. *Nat Commun* **10**, 1523, doi:10.1038/s41467-019-09234-6 (2019).

71 Hughes, C. S. *et al.* Single-pot, solid-phase-enhanced sample preparation for proteomics experiments. *Nat Protoc* **14**, 68-85, doi:10.1038/s41596-018-0082-x (2019).

72 Humphrey, S. J., Karayel, O., James, D. E. & Mann, M. High-throughput and high-sensitivity phosphoproteomics with the EasyPhos platform. *Nat Protoc* **13**, 1897-1916, doi:10.1038/s41596-018-0014-9 (2018).

73 Bruderer, R. *et al.* Extending the limits of quantitative proteome profiling with data-independent acquisition and application to acetaminophen-treated three-dimensional liver microtissues. *Mol Cell Proteomics* **14**, 1400-1410, doi:10.1074/mcp.M114.044305 (2015).

74 Tyanova, S. *et al.* The Perseus computational platform for comprehensive analysis of (prote)omics data. *Nat Methods* **13**, 731-740, doi:10.1038/nmeth.3901 (2016).
75 Bekker-Jensen, D. B. *et al.* Rapid and site-specific deep phosphoproteome profiling by data-independent acquisition without the need for spectral libraries. *Nat Commun* **11**, 787, doi:10.1038/s41467-020-14609-1 (2020).
76 Peronnet, F. & Massicotte, D. Table of nonprotein respiratory quotient: an update. *Can J Sport Sci* **16**, 23-29 (1991).
77 Miotto, P. M. & Holloway, G. P. In the absence of phosphate shuttling, exercise reveals the in vivo importance of creatine-independent mitochondrial ADP transport. *Biochem J* **473**, 2831-2843, doi:10.1042/BCJ20160373 (2016).
78 Yang, C. H. *et al.* Neuropeptide Y1 receptor antagonism protects beta-cells and improves glycemic control in type 2 diabetes. *Mol Metab* **55**, 101413, doi:10.1016/j.molmet.2021.101413 (2022).
79 Mason, R. R. *et al.* PLIN5 deletion remodels intracellular lipid composition and causes insulin resistance in muscle. *Mol Metab* **3**, 652-663, doi:10.1016/j.molmet.2014.06.002 (2014).
80 Dodd, G. T. *et al.* Intranasal Targeting of Hypothalamic PTP1B and TCPTP Reinstates Leptin and Insulin Sensitivity and Promotes Weight Loss in Obesity. *Cell Rep* **28**, 2905-2922 e2905, doi:10.1016/j.celrep.2019.08.019 (2019).
81 Bandyopadhyay, G. K., Yu, J. G., Ofrecio, J. & Olefsky, J. M. Increased malonyl-CoA levels in muscle from obese and type 2 diabetic subjects lead to decreased fatty acid oxidation and increased lipogenesis; thiazolidinedione treatment reverses these defects. *Diabetes* **55**, 2277-2285, doi:10.2337/db06-0062 (2006).
82 Jain, S. S. *et al.* Additive effects of insulin and muscle contraction on fatty acid transport and fatty acid transporters, FAT/CD36, FABPpm, FATP1, 4 and 6. *FEBS Lett* **583**, 2294-2300, doi:10.1016/j.febslet.2009.06.020 (2009).
83 Stahl, A., Evans, J. G., Pattel, S., Hirsch, D. & Lodish, H. F. Insulin causes fatty acid transport protein translocation and enhanced fatty acid uptake in adipocytes. *Dev Cell* **2**, 477-488, doi:10.1016/s1534-5807(02)00143-0 (2002).
84 Perez-Riverol, Y. *et al.* The PRIDE database and related tools and resources in 2019: improving support for quantification data. *Nucleic Acids Res* **47**, D442-D450, doi:10.1093/nar/gky1106 (2019).

Fig. 1

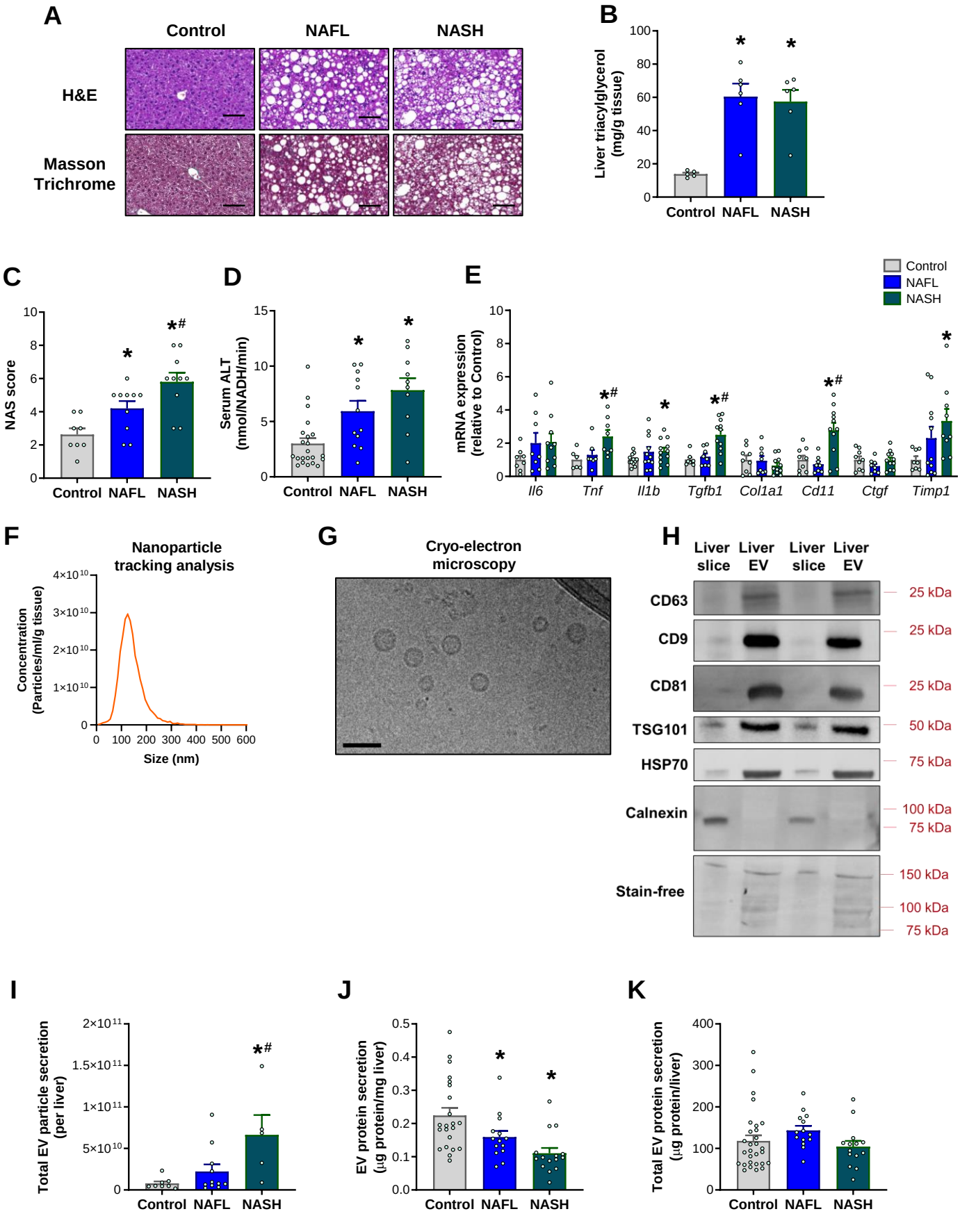
A
Control
NAFL
NASH
H&E
Masson Trichrome
B
Liver triacylglycerol (mg/g tissue)
Control NAFL NASH
C
NAS score
Control NAFL NASH
D
Serum ALT (nmol/NADH/min)
Control NAFL NASH
E
Control
NAFL
NASH
mRNA expression (relative to Control)
Il6 Tnf Il1b Tgfb1 Col1a1 Cd11 Ctgf Timp1
F
Nanoparticle tracking analysis
Concentration (Particles/ml/g tissue)
Size (nm)
G
Cryo-electron microscopy
H
Liver slice
Liver EV
Liver slice
Liver EV
CD63
CD9
CD81
TSG101
HSP70
Calnexin
Stain-free
25 kDa
25 kDa
25 kDa
50 kDa
75 kDa
100 kDa
75 kDa
150 kDa
100 kDa
75 kDa
I
Total EV particle secretion (per liver)
Control NAFL NASH
J
EV protein secretion (µg protein/mg liver)
Control NAFL NASH
K
Total EV protein secretion (µg protein/liver)
Control NAFL NASH

Fig. 2

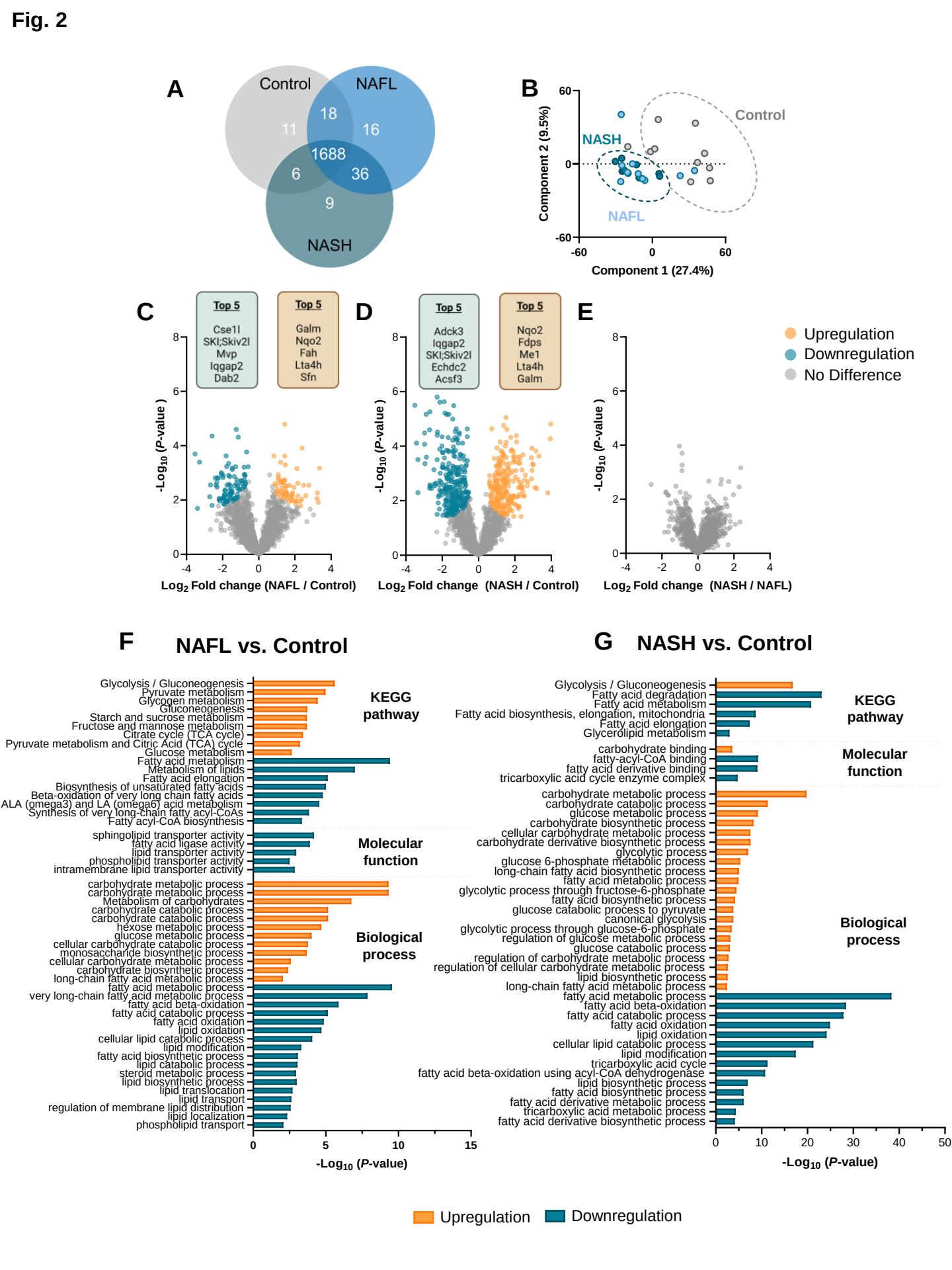
A
Control
NAFL
NASH
18
11
16
1688
6
36
9
B
Control
NASH
NAFL
Component 2 (9.5%)
Component 1 (27.4%)
C
Top 5
Cse1l
SKI;Skiv2l
Mvp
Iqgap2
Dab2
Top 5
Galm
Nqo2
Fah
Lta4h
Sfn
-Log10 (P-value)
Log2 Fold change (NAFL / Control)
D
Top 5
Adck3
Iqgap2
SKI;Skiv2l
Echdc2
Acsf3
Top 5
Nqo2
Fdps
Me1
Lta4h
Galm
Log2 Fold change (NASH / Control)
E
Log2 Fold change (NASH / NAFL)
Upregulation
Downregulation
No Difference
F
NAFL vs. Control
Glycolysis / Gluconeogenesis
Pyruvate metabolism
Glycogen metabolism
Gluconeogenesis
Starch and sucrose metabolism
Fructose and mannose metabolism
Citrate cycle (TCA cycle)
Pyruvate metabolism and Citric Acid (TCA) cycle
Glucose metabolism
Fatty acid metabolism
Metabolism of lipids
Fatty acid elongation
Biosynthesis of unsaturated fatty acids
Beta-oxidation of very long chain fatty acids
ALA (omega3) and LA (omega6) acid metabolism
Synthesis of very long-chain fatty acyl-CoAs
Fatty acyl-CoA biosynthesis
KEGG pathway
sphingolipid transporter activity
fatty acid ligase activity
lipid transporter activity
phospholipid transporter activity
intramembrane lipid transporter activity
Molecular function
carbohydrate metabolic process
carbohydrate metabolic process
Metabolism of carbohydrates
carbohydrate catabolic process
carbohydrate catabolic process
hexose metabolic process
glucose metabolic process
cellular carbohydrate catabolic process
monosaccharide biosynthetic process
cellular carbohydrate metabolic process
carbohydrate biosynthetic process
long-chain fatty acid metabolic process
fatty acid metabolic process
very long-chain fatty acid metabolic process
fatty acid beta-oxidation
fatty acid catabolic process
fatty acid oxidation
lipid oxidation
cellular lipid catabolic process
lipid modification
fatty acid biosynthetic process
lipid catabolic process
steroid metabolic process
lipid biosynthetic process
lipid translocation
lipid transport
regulation of membrane lipid distribution
lipid localization
phospholipid transport
Biological process
-Log10 (P-value)
G
NASH vs. Control
Glycolysis / Gluconeogenesis
Fatty acid degradation
Fatty acid metabolism
Fatty acid biosynthesis, elongation, mitochondria
Fatty acid elongation
Glycerolipid metabolism
KEGG pathway
carbohydrate binding
fatty-acyl-CoA binding
fatty acid derivative binding
tricarboxylic acid cycle enzyme complex
Molecular function
carbohydrate metabolic process
carbohydrate catabolic process
glucose metabolic process
carbohydrate biosynthetic process
cellular carbohydrate metabolic process
carbohydrate derivative biosynthetic process
glycolytic process
glucose 6-phosphate metabolic process
long-chain fatty acid biosynthetic process
fatty acid metabolic process
glycolytic process through fructose-6-phosphate
fatty acid biosynthetic process
glucose catabolic process to pyruvate
canonical glycolysis
glycolytic process through glucose-6-phosphate
regulation of glucose metabolic process
glucose catabolic process
regulation of carbohydrate metabolic process
regulation of cellular carbohydrate metabolic process
lipid biosynthetic process
long-chain fatty acid metabolic process
fatty acid metabolic process
fatty acid beta-oxidation
fatty acid catabolic process
fatty acid oxidation
lipid oxidation
cellular lipid catabolic process
lipid modification
tricarboxylic acid cycle
fatty acid beta-oxidation using acyl-CoA dehydrogenase
lipid biosynthetic process
fatty acid biosynthetic process
fatty acid derivative metabolic process
tricarboxylic acid metabolic process
fatty acid derivative biosynthetic process
Biological process
-Log10 (P-value)
Upregulation
Downregulation

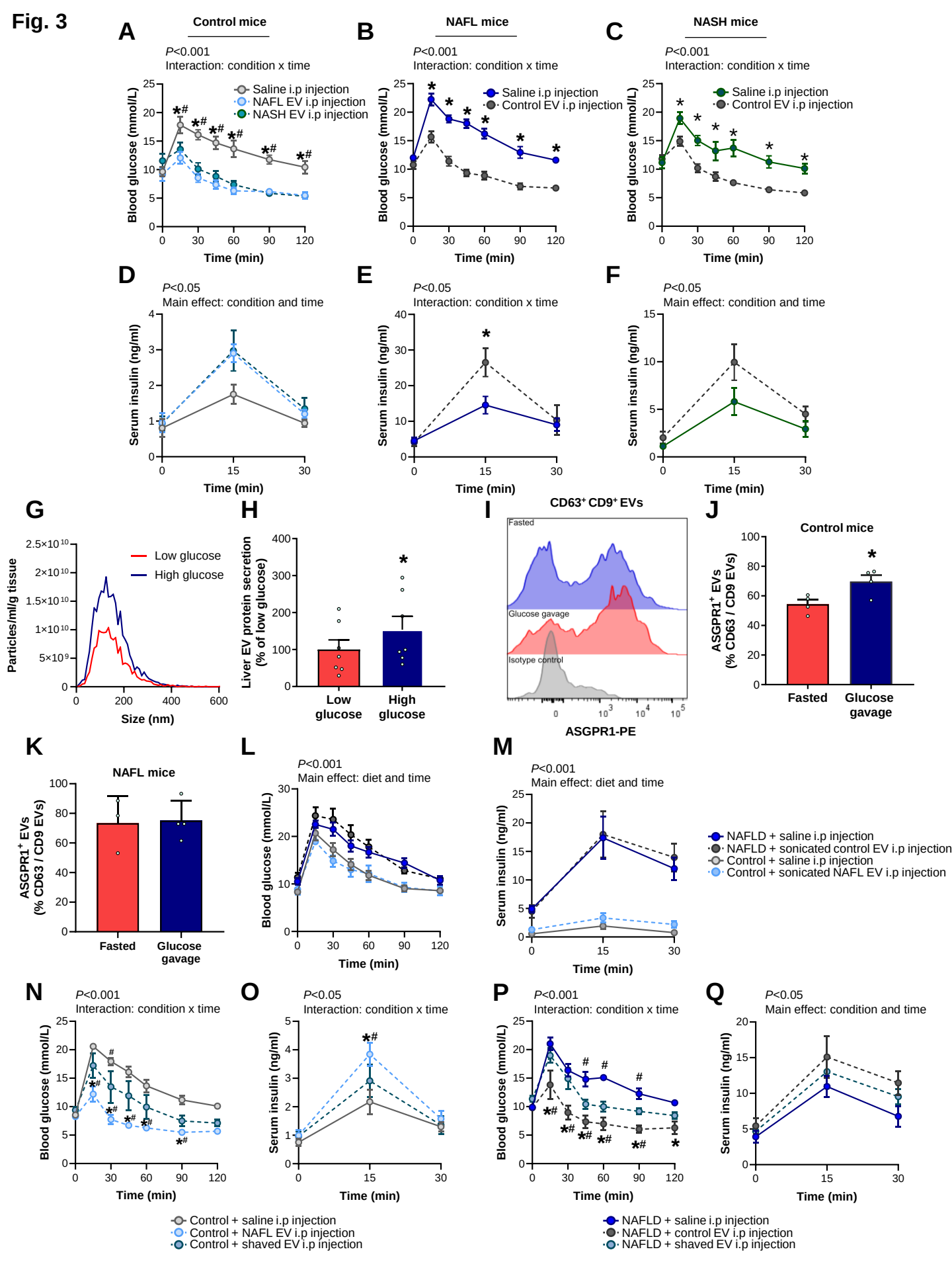
Fig. 3
A
Control mice
P<0.001
Interaction: condition x time
Saline i.p injection
NAFL EV i.p injection
NASH EV i.p injection
Blood glucose (mmol/L)
Time (min)
B
NAFL mice
P<0.001
Interaction: condition x time
Saline i.p injection
Control EV i.p injection
Blood glucose (mmol/L)
Time (min)
C
NASH mice
P<0.001
Interaction: condition x time
Saline i.p injection
Control EV i.p injection
Blood glucose (mmol/L)
Time (min)
D
P<0.05
Main effect: condition and time
Serum insulin (ng/ml)
Time (min)
E
P<0.05
Interaction: condition x time
Serum insulin (ng/ml)
Time (min)
F
P<0.05
Main effect: condition and time
Serum insulin (ng/ml)
Time (min)
G
Low glucose
High glucose
Particles/ml/g tissue
Size (nm)
H
Liver EV protein secretion (% of low glucose)
Low glucose
High glucose
I
CD63+ CD9+ EVs
Fasted
Glucose gavage
Isotype control
ASGPR1-PE
J
Control mice
ASGPR1+ EVs (% CD63 / CD9 EVs)
Fasted
Glucose gavage
K
NAFL mice
ASGPR1+ EVs (% CD63 / CD9 EVs)
Fasted
Glucose gavage
L
P<0.001
Main effect: diet and time
Blood glucose (mmol/L)
Time (min)
M
P<0.001
Main effect: diet and time
Serum insulin (ng/ml)
Time (min)
NAFLD + saline i.p injection
NAFLD + sonicated control EV i.p injection
Control + saline i.p injection
Control + sonicated NAFL EV i.p injection
N
P<0.001
Interaction: condition x time
Blood glucose (mmol/L)
Time (min)
O
P<0.05
Interaction: condition x time
Serum insulin (ng/ml)
Time (min)
P
P<0.001
Interaction: condition x time
Blood glucose (mmol/L)
Time (min)
Q
P<0.05
Main effect: condition and time
Serum insulin (ng/ml)
Time (min)
Control + saline i.p injection
Control + NAFL EV i.p injection
Control + shaved EV i.p injection
NAFLD + saline i.p injection
NAFLD + control EV i.p injection
NAFLD + shaved EV i.p injection

Fig. 4

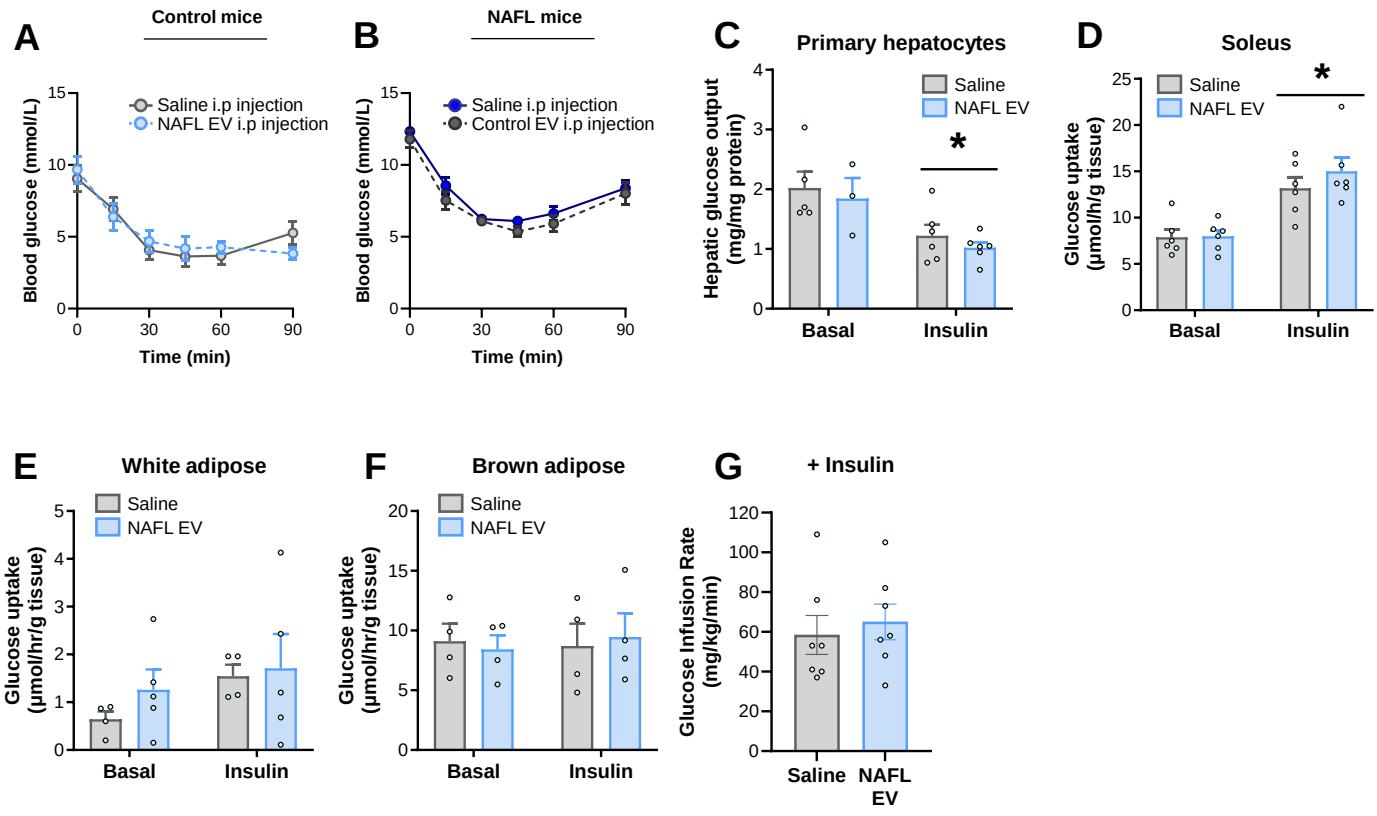
A
Control mice
Saline i.p injection
NAFL EV i.p injection
Blood glucose (mmol/L)
Time (min)
B
NAFL mice
Saline i.p injection
Control EV i.p injection
Blood glucose (mmol/L)
Time (min)
C
Primary hepatocytes
Saline
NAFL EV
Hepatic glucose output (mg/mg protein)
Basal
Insulin
D
Soleus
Saline
NAFL EV
Glucose uptake (µmol/hr/g tissue)
Basal
Insulin
E
White adipose
Saline
NAFL EV
Glucose uptake (µmol/hr/g tissue)
Basal
Insulin
F
Brown adipose
Saline
NAFL EV
Glucose uptake (µmol/hr/g tissue)
Basal
Insulin
G
+ Insulin
Glucose Infusion Rate (mg/kg/min)
Saline
NAFL EV

Fig. 5

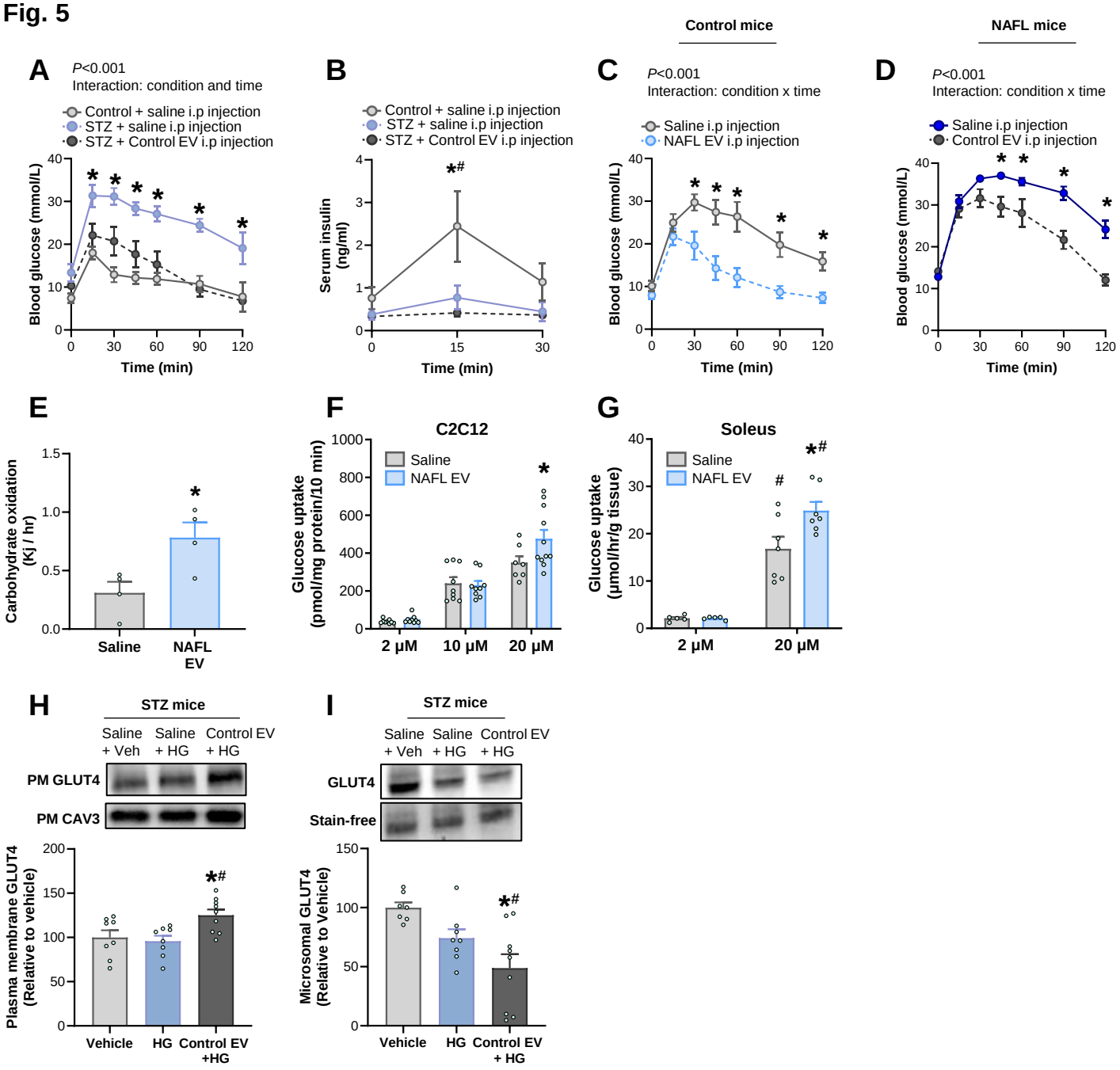
Control mice
NAFL mice
A
P<0.001
Interaction: condition and time
Control + saline i.p injection
STZ + saline i.p injection
STZ + Control EV i.p injection
Blood glucose (mmol/L)
Time (min)
B
Control + saline i.p injection
STZ + saline i.p injection
STZ + Control EV i.p injection
Serum insulin (ng/ml)
Time (min)
C
P<0.001
Interaction: condition x time
Saline i.p injection
NAFL EV i.p injection
Blood glucose (mmol/L)
Time (min)
D
P<0.001
Interaction: condition x time
Saline i.p injection
Control EV i.p injection
Blood glucose (mmol/L)
Time (min)
E
Carbohydrate oxidation (Kj / hr)
Saline
NAFL EV
F
C2C12
Saline
NAFL EV
Glucose uptake (pmol/mg protein/10 min)
2 µM
10 µM
20 µM
G
Soleus
Saline
NAFL EV
Glucose uptake (µmol/hr/g tissue)
2 µM
20 µM
H
STZ mice
Saline + Veh
Saline + HG
Control EV + HG
PM GLUT4
PM CAV3
Plasma membrane GLUT4 (Relative to vehicle)
Vehicle
HG
Control EV +HG
I
STZ mice
Saline + Veh
Saline + HG
Control EV + HG
GLUT4
Stain-free
Microsomal GLUT4 (Relative to Vehicle)
Vehicle
HG
Control EV + HG

Fig. 6

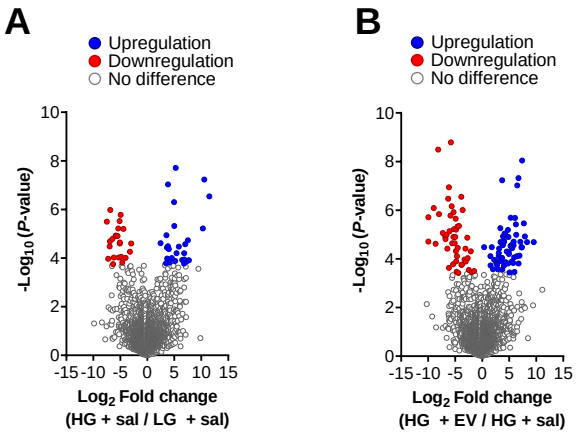

C

Downregulated phosphosites (HG + saline / LG + saline)	Downregulated phosphosites (HG + EV / HG + saline)	
Actn3_S610	Aak1_S650	Myot_S227
Ankrd17_S1934	Arhgef11_T1462	Myo9b_S1326
Asb2_S72	Arhgef11_T1463	Naca_T1169
CEFIP_S675	Bag3_S289	Pcyt1a_T342
Cmya5_S1179	Birc6_S485	Pip4P2_S33
Dync1li1_S516	Cic_S2311	Plec_S4620
Gsk3a_Y279	Ckmt2_S319	Plec_S4625
H2-D1, H2-L_S361	Crtc3_S62	Plec_T19
Hdlbp_T28	Dmtn_S96	Popdc2_S272
Hsp90ab1_S445	Dtd1_S194	Ppp1r12b_T726
Larp4b_S603	Exoc1_S455	**Prob1_S451**
Myom3_S265	Esyt2_S662	Ptges3l_S147
Naca_T1395	Fam8a1_S27	Shank3_S373
Niban1_T583	Fxr1_T512	Shank3_S387
Pdlim3_T132	Fxr1_S514	Slc23a2_S78
Ppp1r3a_S51	Gapvd1_S338	Sptbn1_S2160
Prob1_S396	Inf2_S628	Tacc2_S2213
Prob1_S398	Inf2_S630	Tbc1d5_S583
Prob1_S407	Itgb4_S1358	Tceal3, Tceal5,
Svil_S328	Jcad_S1248	Tceal6_T117
Svil_S335	Lipe_S870	Tjp1_T379
Tns1_S1427	Lrch1_S522	Trim72_S188
Tomm70_S105	Lrch1_T524	**Tns1_S963**
	Mapt_S487	Usp47_S832
	Myh7_T1519	

D

Upregulated phosphosites (HG + saline / LG + saline)	Upregulated phosphosites (HG + EV / HG + saline)	
Arhgef11_T1463	Ablim3_S282	Ptprg_S404
Camk2b_S397	Abra_S147	Pxn_S591
Cav2_T5	Acin1_S156	Ranbp3_S217
Cdk12_S275	Afdn_S1157	Rcsd1_S120
CEFIP_S515	Ank3_S752	Relch_S186
CEFIP_S518	Asb2_S72	Relch_S180
Cmya5_S1019	Atxn2l_S333	Retreg3_S320
Fundc1_Y11	**Camk2b_T400**	Rreb1_S1612
Fxr1_T512	Camsap2_S450	Sfswap_S283
Fxr1_S514	Coro6_S382	Sp1_S2
Hspa12b_S25	Dnajc5_T11	Speg_S2187
Itgb4_S1358	Dync1li1_S516	Speg_S2322
Mtus1_S425	Farp1_T24	Sptan1_S1530
Myh7_T1519	Flnc_S2204	Sptan1_T1532
Myoz1_S260	Jph2_T174	Srrm2_S1498
Naca_S1914	Larp1_S604	Srrm2_S1646
Pcif1_S30	Larp4b_S603	Stim1_S524
Pdha1_S295	Limch1_S592	Stxbp5_S745
Ppfia1_S238	Lmnb1_S159	Svil_S321
Raph1_S899	Map3k20_T323	Svil_S328
Smtnl1_T179	Mavs_S152	Synpo_T547
Srl_S304	Mybpc1_S715	Synpo2_S759
Tbc1d5_S583	Myh1_S1343	Tbc1d15_S662
Trim72_S188	Myh2_S1291	Ttn_T34192
Ubxn1_T157	**Naca_S1491**	Ube4b_S31
Ubxn1_S165	**Pdha1_S300**	Uhrf1bp1_S914
Ube2z_S341	Plcb4_T886	Uts2r_S343
	Plcb4_S889	Vcan_S2578
	Ppp1r3a_S51	Wnk1_S172
	Prkag2_S196	Zeb1_S663
	Ptpn12_S606	

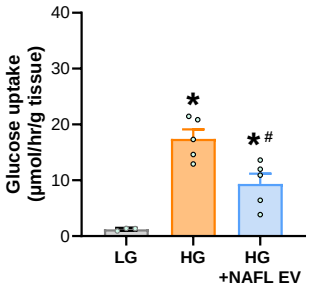

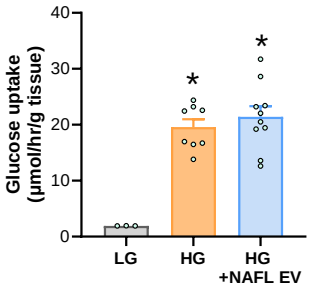

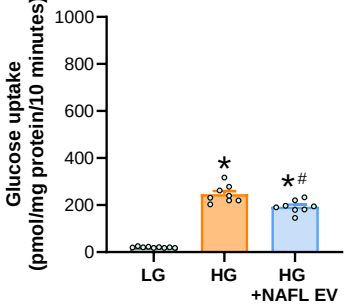

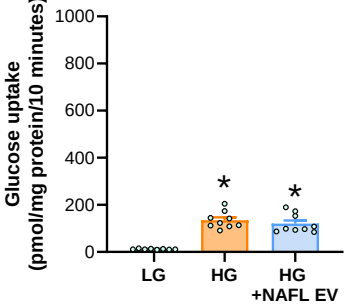

Fig. 7

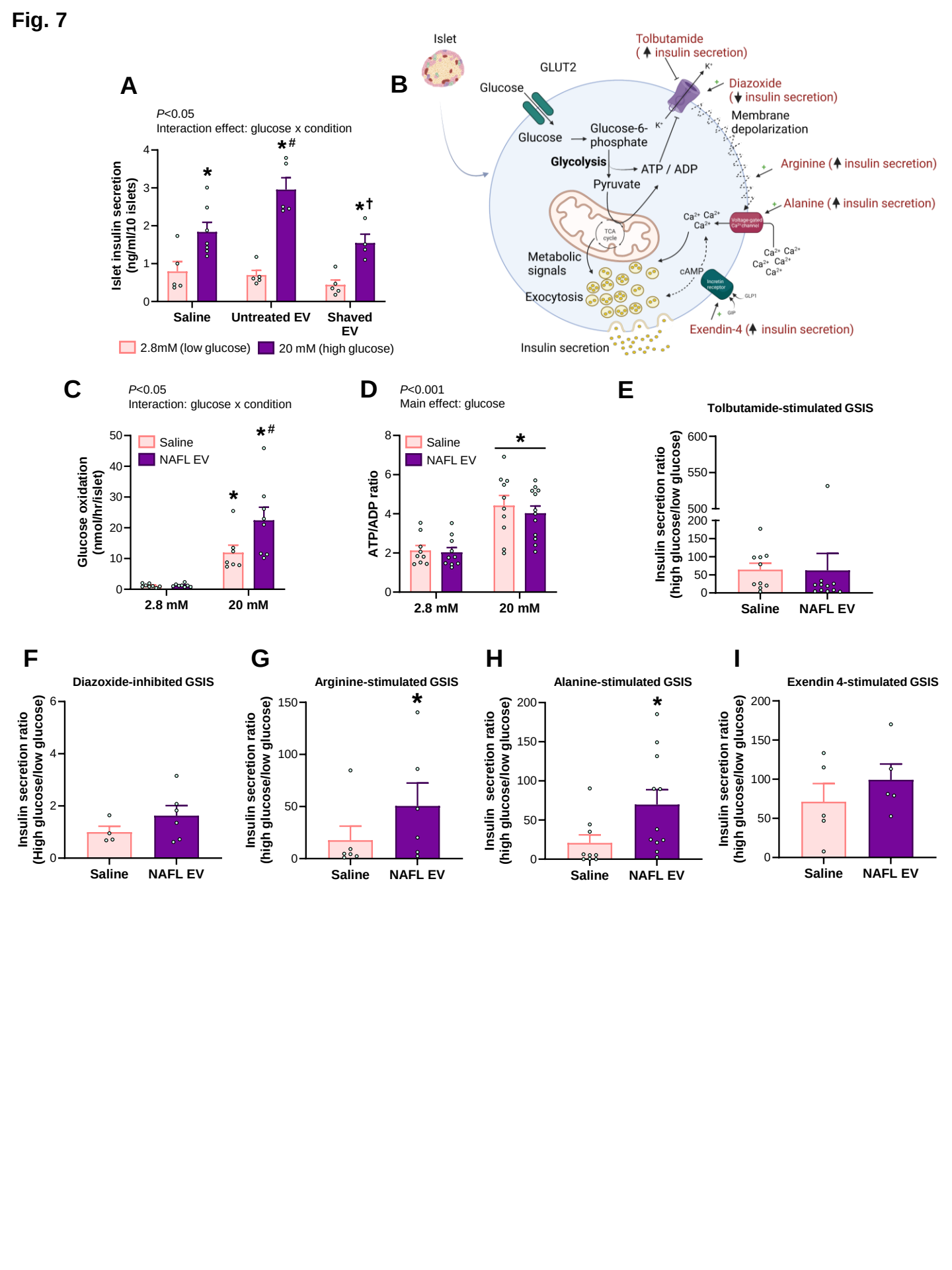
A
P<0.05
Interaction effect: glucose x condition
Islet insulin secretion (ng/ml/10 islets)
Saline
Untreated EV
Shaved EV
2.8mM (low glucose)
20 mM (high glucose)
B
Islet
GLUT2
Glucose
Glucose
Glucose-6-phosphate
Glycolysis
ATP / ADP
Pyruvate
TCA cycle
Metabolic signals
Exocytosis
Insulin secretion
Tolbutamide (insulin secretion)
Diazoxide (insulin secretion)
Membrane depolarization
Arginine (insulin secretion)
Alanine (insulin secretion)
cAMP
Exendin-4 (insulin secretion)
C
P<0.05
Interaction: glucose x condition
Glucose oxidation (nmol/hr/islet)
Saline
NAFL EV
2.8 mM
20 mM
D
P<0.001
Main effect: glucose
ATP/ADP ratio
Saline
NAFL EV
2.8 mM
20 mM
E
Tolbutamide-stimulated GSIS
Insulin secretion ratio (high glucose/low glucose)
Saline
NAFL EV
F
Diazoxide-inhibited GSIS
Insulin secretion ratio (High glucose/low glucose)
Saline
NAFL EV
G
Arginine-stimulated GSIS
Insulin secretion ratio (high glucose/low glucose)
Saline
NAFL EV
H
Alanine-stimulated GSIS
Insulin secretion ratio (high glucose/low glucose)
Saline
NAFL EV
I
Exendin 4-stimulated GSIS
Insulin secretion ratio (high glucose/low glucose)
Saline
NAFL EV

Fig. 8

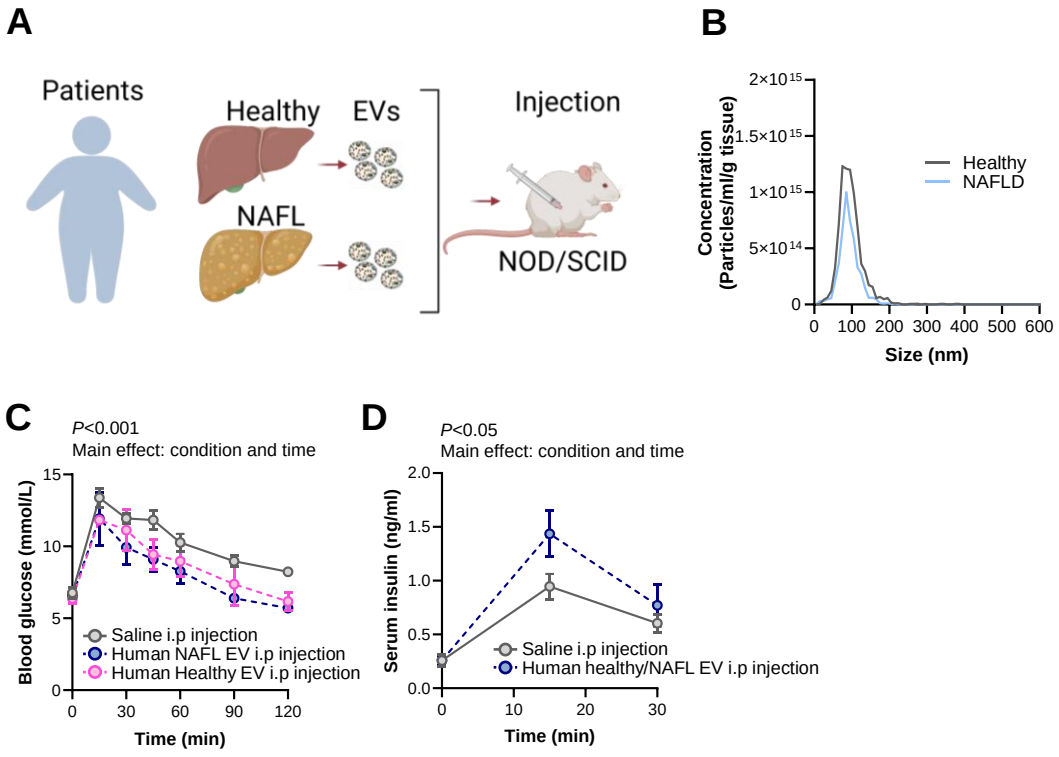
A
Patients
Healthy
EVs
NAFL
Injection
NOD/SCID
B
Concentration (Particles/ml/g tissue)
2×10^15
1.5×10^15
1×10^15
5×10^14
0
Healthy
NAFLD
0 100 200 300 400 500 600
Size (nm)
C
P<0.001
Main effect: condition and time
Blood glucose (mmol/L)
15
10
5
0
Saline i.p injection
Human NAFL EV i.p injection
Human Healthy EV i.p injection
0 30 60 90 120
Time (min)
D
P<0.05
Main effect: condition and time
Serum insulin (ng/ml)
2.0
1.5
1.0
0.5
0.0
Saline i.p injection
Human healthy/NAFL EV i.p injection
0 10 20 30
Time (min)

Extended data Fig. 1

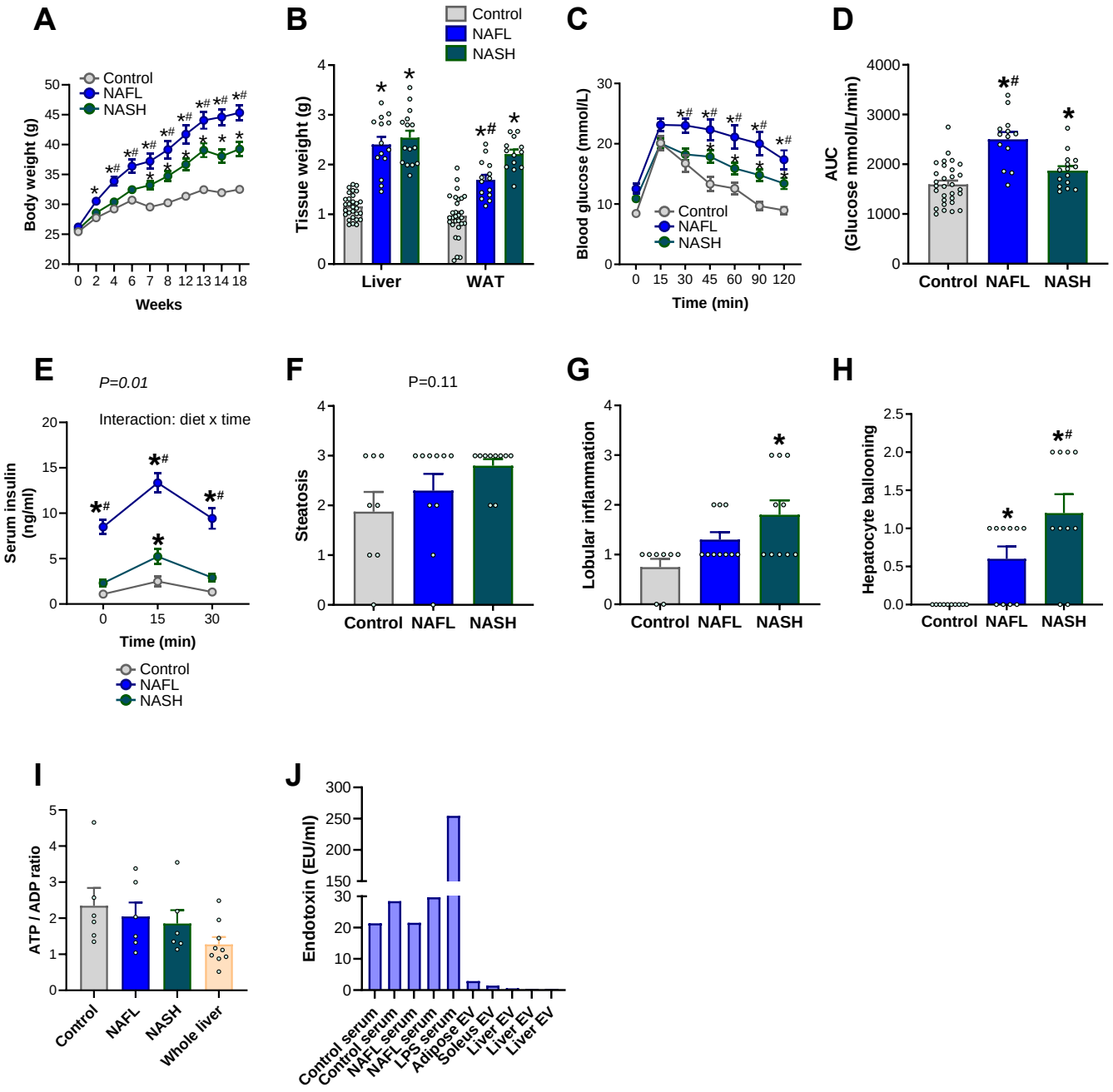

Extended data Fig. 1. Characteristics of diet-induced glucose intolerance and extracellular vesicle purity.

(A) Body weight over 20 weeks consumption of control (n=30), NAFL (n=15), and NASH diet (n=15) across 1 cohort. *, significant from Control; #, significant from NASH. *P*<0.001.

(B) Liver and epididymal (EWAT) tissue mass in response to Control (n=29), NAFL (n=14), or NASH (n=15 liver, n=13 EWAT) across 1 cohort. *, significant from Control; #, significant from NASH. *P*<0.001.

(C-D) Blood glucose levels during an oral glucose tolerance test (2 g/kg) (C) and the corresponding glucose area under the curve (AUC; D) of mice fed different dietary interventions (n=15 control, n=9 NAFL, n=13 NASH) across 1 cohort. *, significant from Control; #, significant from NASH. *P*<0.001.

(E) Serum insulin during the oral glucose tolerance test (n=5 control, n=9 NAFL, n=9 NASH) across 1 experiment. *, significant from Control; #, significant from NASH. *P*=0.01.

(F) Steatosis score in Control (n=8), NAFL (n=10), and NASH (n=10) livers derived from histopathology across 1 cohort. *P*=0.1.

(G) Lobular inflammation score in Control (n=8), NAFL (n=10), and NASH (n=10) livers derived from histopathology across 1 cohort. *P*=0.017.

(H) Hepatocyte ballooning score in Control, NAFL, and NASH livers derived from histopathology (n=8 control, n=10 NAFL, n=10 NASH) across 1 cohort. *, significant from Control; #, significant from NAFL. *P*<0.001.

(I) ATP / ADP ratio in liver slices and whole liver from Control, NAFL, and NASH mice (n=6/group for liver slices, n=9 for whole liver pooled from Control, NAFL, and NASH mice) across 1 experiment. *P*=0.07.

(J) Endotoxin levels in the circulation and in extracellular vesicle (EV) preparations (each bar represents an individual biological sample) across 1 experiment.

Data are expressed as mean ± SEM. Each datapoint represents an independent biological sample. Data was analysed using a repeated measures two-way ANOVA (A, C, E) or one-way ANOVA (B (EWAT), D, F, H, I) followed by a Student Newman Keuls post-hoc, or Kruskal Wallis one-way ANOVA on ranks (B (liver), G) followed by a Dunn's test.

Extended data Fig. 2

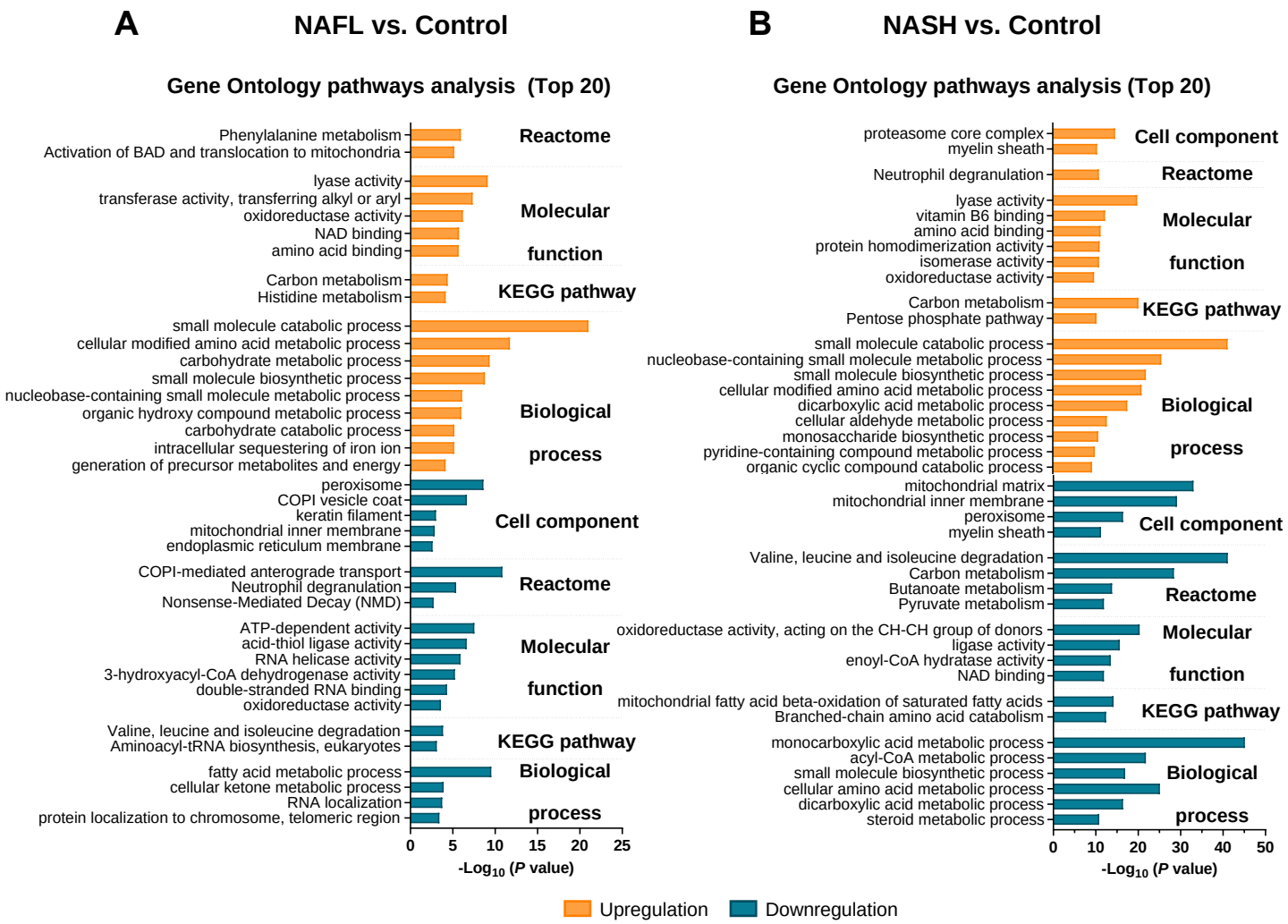

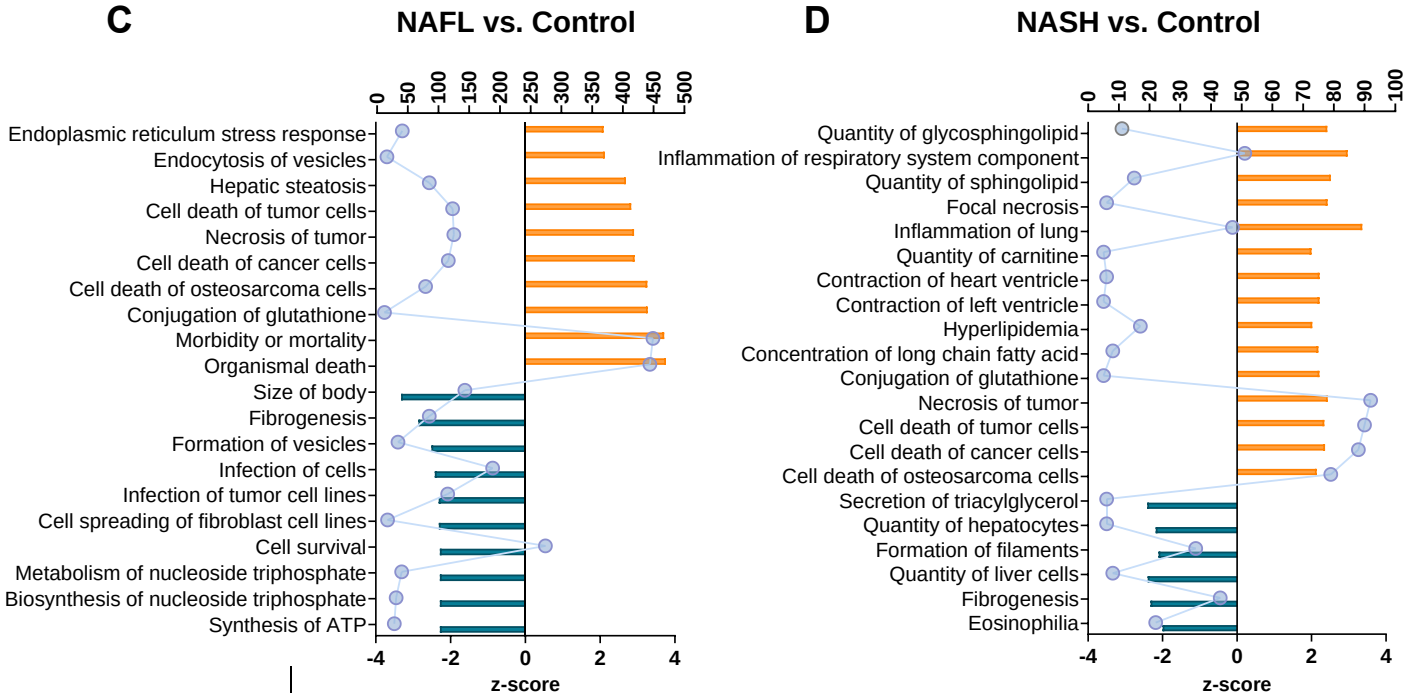

Extended data Fig 2. Pathways analysis of the liver extracellular vesicle proteome in response to NAFL or NASH.

(A-B) Top 20 biological processes identified using pathways enrichment analysis (Metascape.com) in NAFL relative to control conditions (A), and in NASH relative to control conditions (B). n= 10/group. *P* values indicated within figure.

(C-D) Pathway enrichment analysis of disease functions and toxicology using Ingenuity Pathways Analysis in NAFL (C) and NASH (D) compared to healthy control mice. n= 10/group. $P<0.001$. Data represented as z-score or -log10 P-value, derived from proteomics analysis using unpaired two-tailed t-test.

Extended data Fig 3

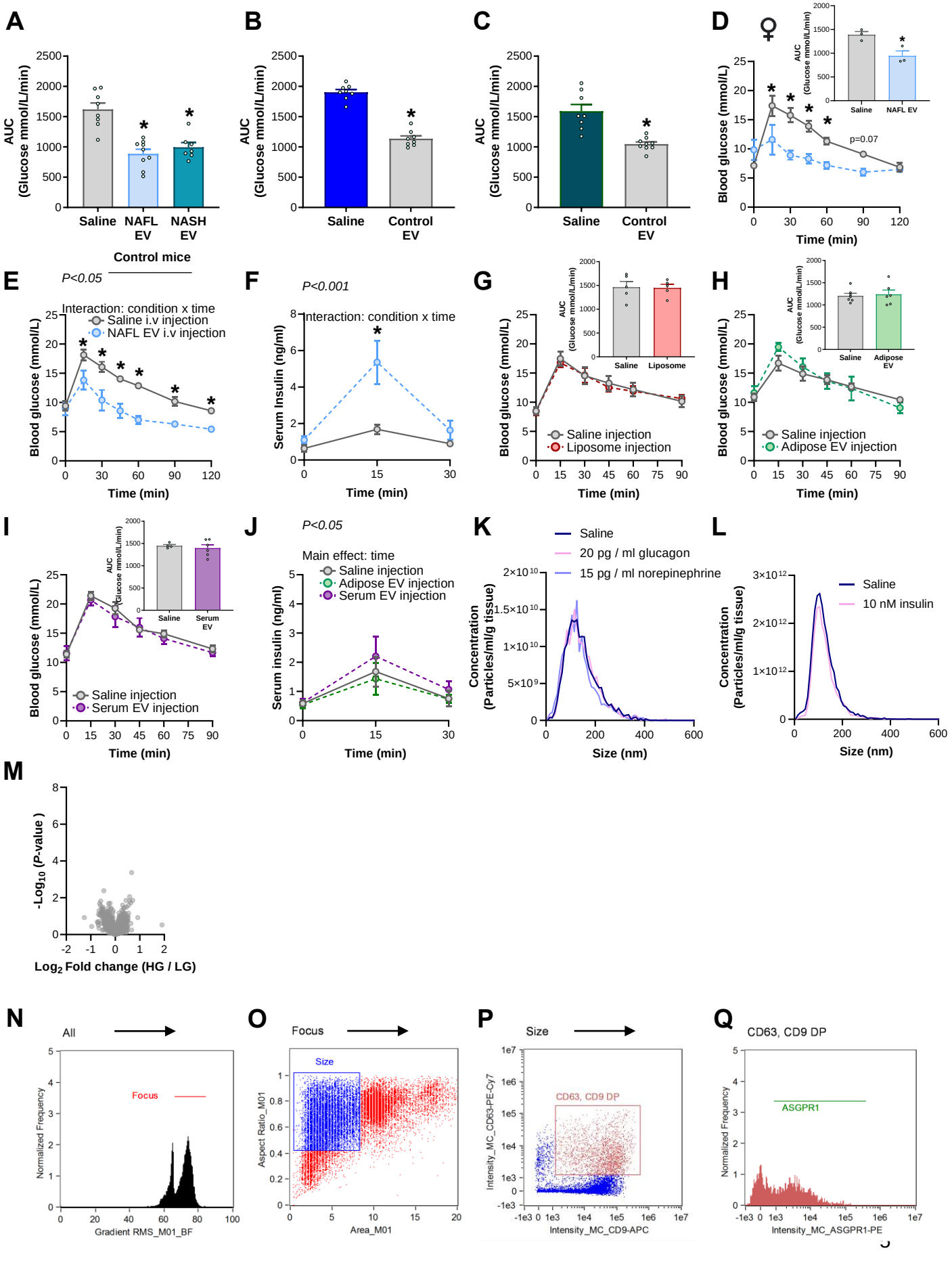

Extended data Fig. 3. Glucose tolerance testing in mice in response to extracellular vesicles derived from various sources and glucose-stimulated extracellular vesicle secretion.

(A-C) The GTT glucose area under the curve (AUC) in control (A, n=8 saline, n=9 NAFL EV, n=7 NASH EV), NAFL (B, n=8/group), or NASH (C, n=8 saline, n=9 Control EV) mice in response to saline or liver EVs across 1 cohort. *P*<0.001. *, significant from Saline.

(D) Blood glucose and AUC during GTT in female mice in response to saline or liver EV (n=3/group) across 1 cohort. *, significant from NAFL EV injection. *P*<0.001, *P*=0.02 (inset).

(E-F) Blood glucose (E, *P*=0.001) and serum insulin (F, *P*<0.001) during GTT in control mice that received i.v injection of saline or liver EV (n=6 saline, n=4 NAFL EV) across 1 cohort. *, significant from NAFL EV injection.

(G-I) Blood glucose levels and the AUC (inset) of Control mice injected intraperitoneally with saline or empty liposomes (G, n=5/group, *P*<0.001 (main effect: Time), *P*=0.91 (inset)), adipose-derived EVs (H, n=7 saline, n=6 adipose EV, *P*<0.001 (main effect: Time), *P*=0.76 (inset)), or serum derived EVs (I, n=4 saline, n=6 serum EV, *P*<0.001 (main effect: Time), *P*=0.603 (inset)) across 2 cohorts.

(J) Serum insulin during an oral GTT in response to administration of saline (n=6), adipose-derived EVs (n=5), or serum EVs (n=5) across 1 experiment. *P*<0.001 (main effect: Time).

(K-L) Nanoparticle-tracking analysis of liver EVs from liver slices in response to high glucose (20 mM), in the absence or presence of (K, *P*=0.994) saline (n=6), glucagon (n=5), or norepinephrine (n=5), and (L, *P*=0.22) saline (n=6) or insulin (n=5) across 1 experiment for each comparison.

(M) Volcano plot comparison of the liver EV proteome secreted by healthy liver slices in response to high glucose (20 mM, n=6) relative to low glucose (2 mM, n=5) across 1 experiment.

(N-Q) Gating strategy for imaging flow cytometry in Control mice (n=4/group) that were fasted and subjected to an oral gavage of water (vehicle) or glucose. The unfocused bright field signals were excluded using Gradient RMS feature (N). Particles with relative area smaller than the speed beads were gated by the discriminating aspect ratio and area of particles (previously optimised) (O). CD63-PE-Cy7 and CD9-APC positive particles were gated (P). ASGPR positive particles were plotted and gated based on the isotype control (Q). 1 independent experiment.

Data are expressed as mean ± SEM. Each datapoint represents an independent biological sample. Data was analysed using a one-way ANOVA (A, K (calculated from AUC), repeated measures two-way ANOVA (D, E, F, G, H, I, J) with Student Newman Keuls post-hoc, or unpaired two-tailed t-test (B, C, D (inset), G (inset), H (inset), I (inset), L (calculated from AUC), M).

Extended data Fig 4

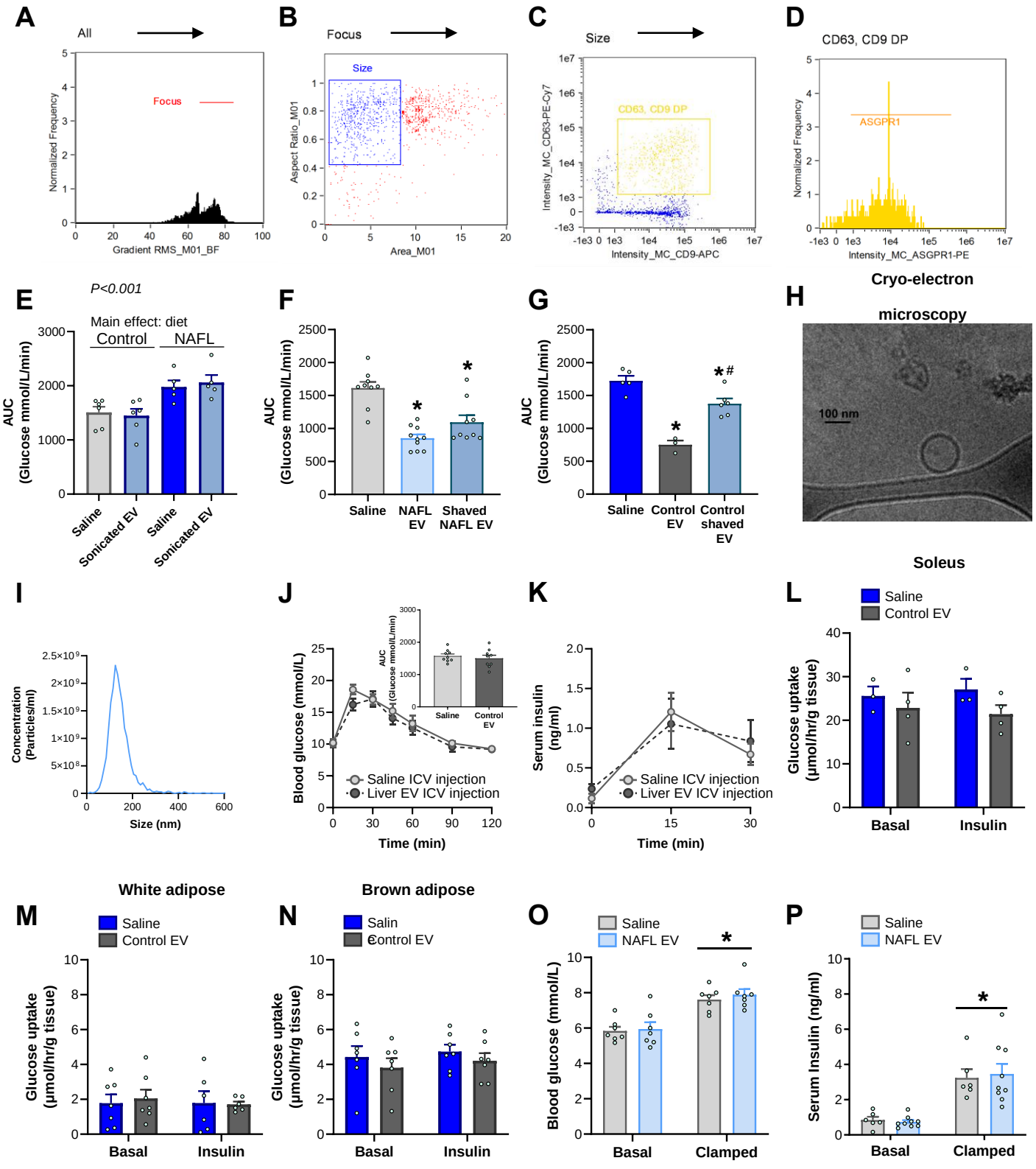

Extended data Fig . 4. Glucose tolerance testing in mice in response to extracellular vesicles derived from various treatments, tissue insulin sensitivity in isolated tissue, and blood glucose and insulin levels during a hyperinsulinemic-euglycemic clamp.

(A-D) Gating strategy for imaging flow cytometry in NAFL mice (n=3 fasted, n=4 glucose gavage) that were fasted and subjected to an oral gavage of water (vehicle) or glucose. The unfocused bright field signals were excluded using Gradient RMS feature (A). Particles with relative area smaller than the speed beads were gated by the discriminating aspect ratio and area of particles (previously optimised) (B). CD63-PE-Cy7 and CD9-APC positive particles were gated (C). ASGPR positive particles were plotted and gated based on the isotype control (D). 1 independent experiment.

(E) Glucose AUC during an oral GTT in Control (n=6/group) and NAFL mice (n=5/group) in response to sonicated liver EVs across 1 cohort. $P<0.001$ (main effect).

(F-G) Glucose AUC during an oral GTT in Control (F, n=9 saline, n=10 NAFL EV, n=9 'shaved EV) or NAFL (G, n=5 saline, n=3 Control EV, n=6 'shaved' EV) mice that received saline or 'shaved' liver EVs across 2 cohorts (control) and 1 cohort (NAFL). $P<0.001$. *, significant from Saline; #, significant from Control EV.

(H) Representative cryo-electron microscopy of 'shaved' liver EV preparation. 1 experiment.

(I) Nanoparticle tracking analysis of 'shaved' liver EV. 1 experiment, n=4 biological replicates graphed as an average.

(J-K) Blood glucose levels and AUC (inset) during an oral GTT (J), and serum insulin (K) of mice that received intracerebral ventricular injection (ICV) of saline/liver EVs during 1 experiment (n=9/group). $P<0.001$ (main effect: time).

(L-N) Glucose uptake in isolated soleus muscle (L, n=3 saline, n=4 Control EV, $P=0.61$, basal and insulin-stimulated samples are paired from the same animal within each treatment), white adipose tissue (M, n=7 saline/basal, n=6 saline/insulin, n=7 Control EV/basal, n=6 Control EV/insulin, $P=0.73$), and brown adipose tissue (N, n=7/group, $P=0.932$) collected from NAFL mice and treated *ex vivo* with saline or liver EVs (10 µg/ml) obtained from healthy Control mice 1 hr prior to and during the experiment. 1 cohort across tissues. Basal and insulin-stimulated samples from adipose are paired from the same animal across both treatments, with exception of 1 mouse for the EWAT comparison (i.e., basal saline vs. basal EV).

(O) Blood glucose levels at baseline (i.e., fasted state) and during a hyperinsulinemic-euglycemic clamp in Control mice (n=7/group) following intraperitoneal injection of NAFL EV 1 hr prior to the experiment. $P<0.001$ (main effect). 1 independent cohort.

(P) Serum insulin at baseline (i.e., fasted state) and during a hyperinsulinemic-euglycemic clamp in Control mice (n=6 saline, 9 NAFL EV) following intraperitoneal injection of NAFL EV 1 hr prior to the experiment. $P<0.001$ (main effect). 1 independent cohort.

Data are expressed as mean ± SEM. Each datapoint represents an independent biological sample. Data was analysed using a one-way ANOVA (F, G), two-way ANOVA (E, L, M, N) or repeated measures two-way ANOVA (J, K, O, P) with Student Newman Keuls post-hoc analyses, or unpaired two-tailed t-test (J (inset)). *, significant main effect compared to basal.

Extended data Fig. 5

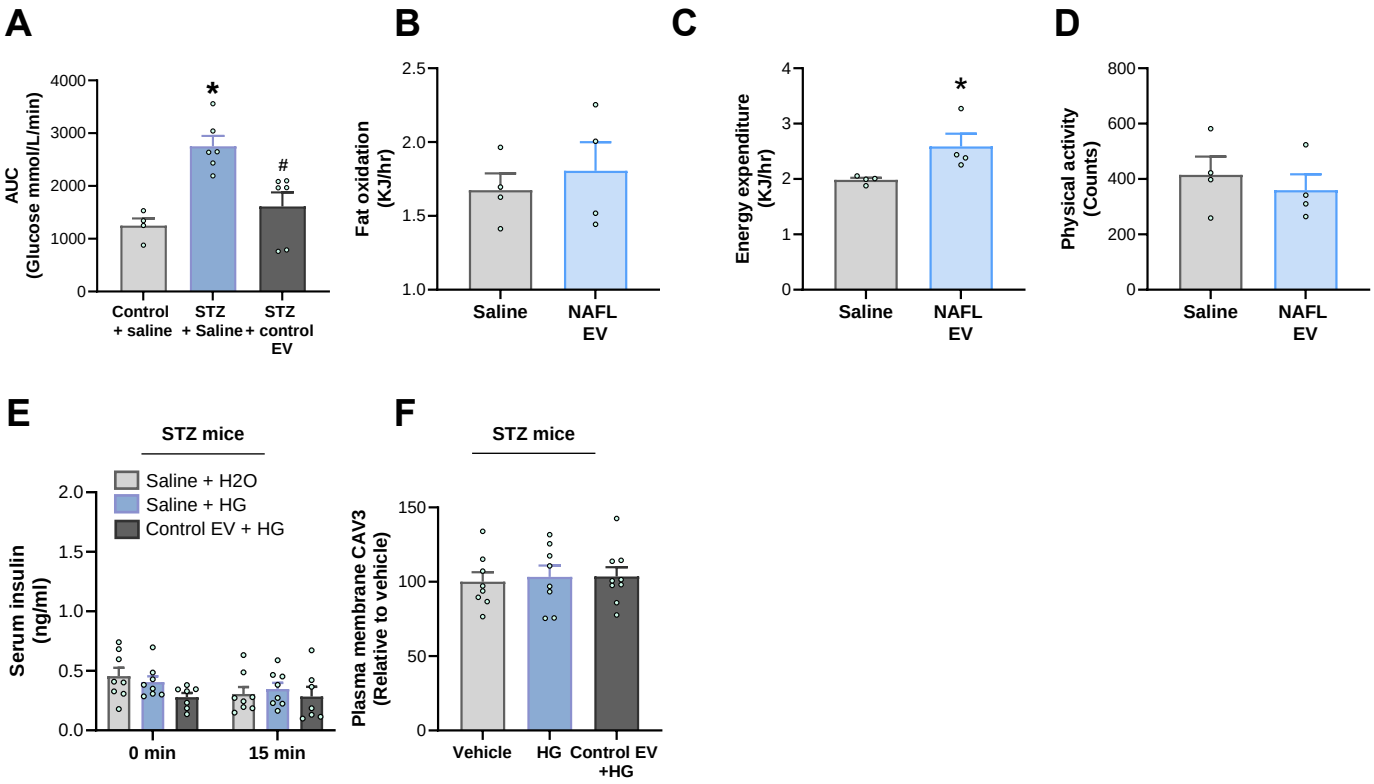

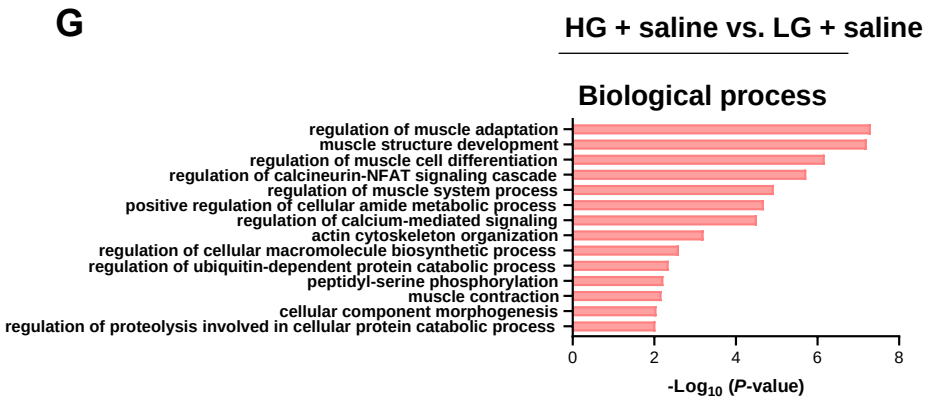

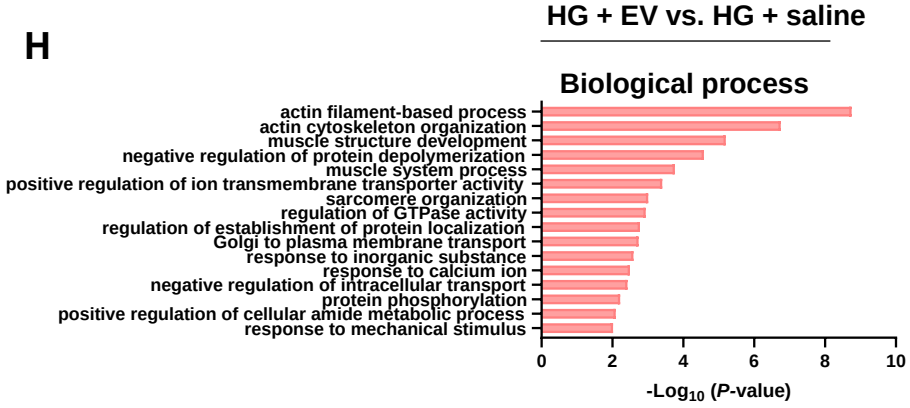

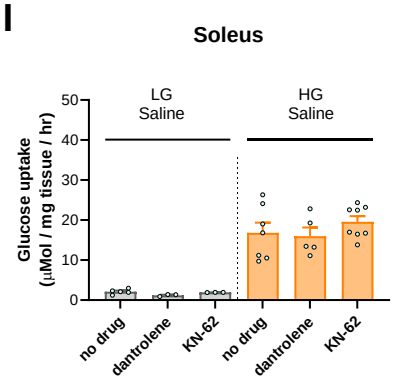

Extended data Fig. 5. Effect of liver extracellular vesicles in regulating glucose effectiveness.

(A) Glucose area under the curve (AUC) during an oral glucose tolerance test in streptozotocin (STZ) treated mice that received an intraperitoneal injection of saline or Control liver EVs (n=4 control saline, n=6/group STZ) across 1 cohort. *, significant from Control + saline; #, significant from STZ + saline. *P*=0.001.

(B-D) Whole body calorimetry and activity in Control mice over 2 hours in response to saline or liver EVs. Fat oxidation (B, *P*=0.58), energy expenditure (C, *P*=0.04), and physical activity (D, *P*=0.54). n=4/group. 1 experiment. *, significant from Saline.

(E) Serum insulin in STZ mice in response to saline or liver EVs, followed by gavage with vehicle (n=8 saline/H2O) or glucose (n=8 saline/high glucose (HG), n=7 liver control EV/HG) 1 hr later across 2 cohorts. *P*=0.245.

(F) Plasma membrane CAV3 content in STZ mice in response to saline or liver EVs followed by oral gavage with vehicle (n=8 saline/H2O) or glucose (n=8 saline/HG, n=9 control EV + HG) 1 hr later across 2 cohorts. *P*=0.918.

(G) Pathways enrichment analysis for phosphosites regulated in soleus muscle from Control mice following high glucose (HG + saline, n=5) treatment relative to low glucose (LG + saline, n=4) in the presence of saline. q<0.05.

(H) Pathways enrichment analysis for phosphosites regulated in soleus muscle from Control mice following high glucose treatment and liver EVs (HG + EV, n=5) relative to HG and saline (HG + saline, n=5). q<0.05.

(I) Glucose uptake between no drug, dantrolene (5 μM), and KN-62 (10 μM) under LG (2 μM, n=5 no drug, n=3 dantrolene, n=3 KN-62) and HG (20 μM, n=7 no drug, n=5 dantrolene, n=8 KN-62) conditions in soleus muscle. *P*<0.001 main effect: condition. Same values reassessed from Fig. 6E and 6F.

Data are expressed as mean ± SEM. Each data point represents an independent biological sample. Data was analysed using one-way ANOVA (A, F) and two- way repeated measures ANOVA (E) with Student Newman Keuls post-hoc, or unpaired two-tailed t-test (B, C, D, G, H).

Extended data Fig 6

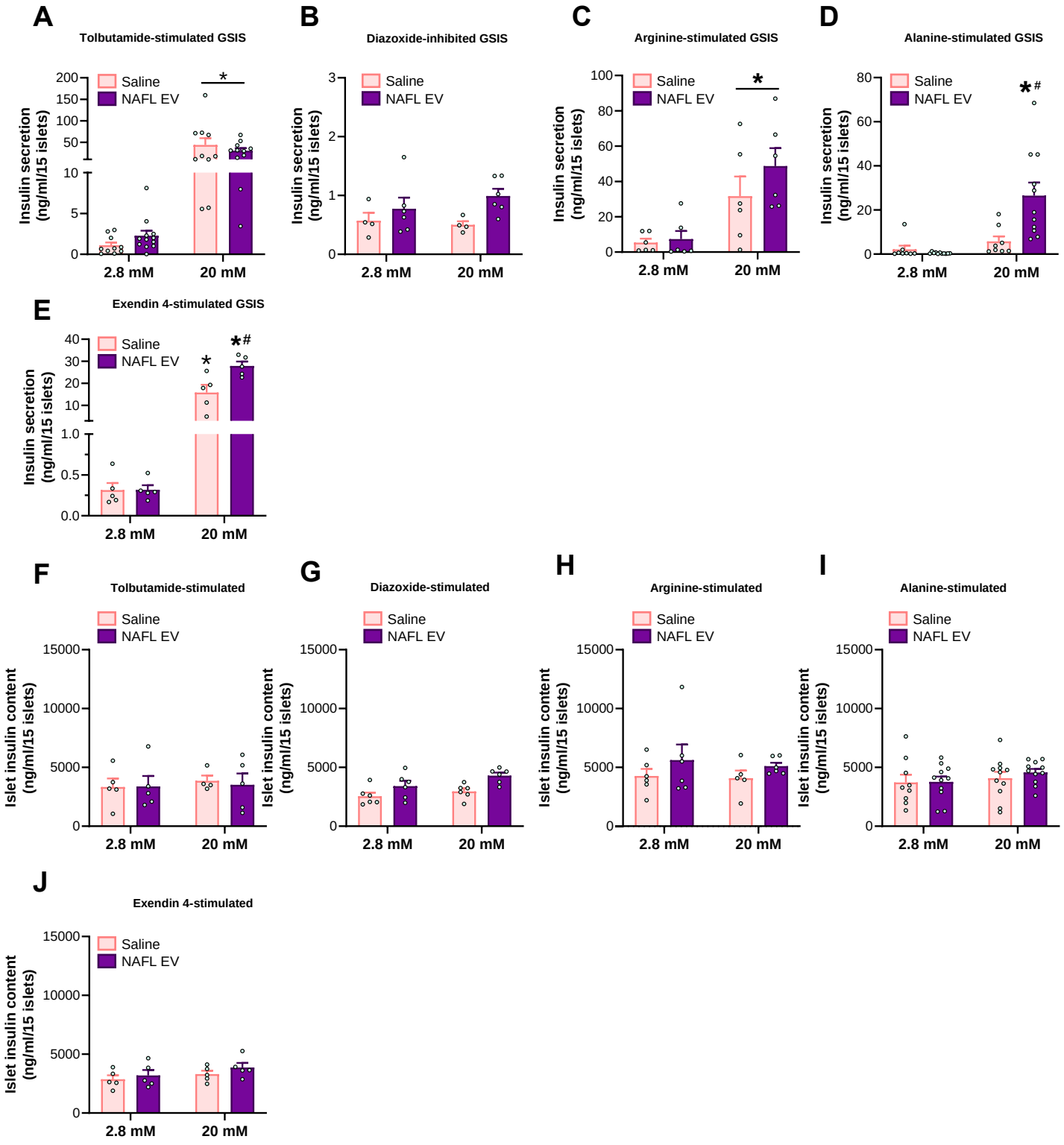

Extended data Fig 6. Effect of liver extracellular vesicles on insulin secretion and cellular insulin content.

(A-E) Glucose-stimulated insulin secretion from isolated healthy murine islets in the presence or absence of NAFL liver EVs (10 µg/ml), when treated with tolbutamide (A, n=10 saline/2.8 mM or 20 mM, n=12 NAFL EV/2.8 mM, n=11 NAFL EV/20 mM, $P<0.001$ (main effect)), diazoxide (B, n=4 saline/group, n=6 NAFL EV/group, $P=0.364$), arginine (C, n=6/group, $P<0.001$ (main effect)), alanine (D, n=8 saline/group, n=11 NAFL EV/group, $P<0.008$), or exendin 4 (E, n=5/group, $P=0.019$) across 2 experiments involving isolations from 9 mice. *, significant from low glucose (2.8 mM) within same condition (i.e., saline or liver EV) or significant main effect of high glucose (20 mM); #, significant from saline within 20 mM glucose condition.

(F-J) Islet insulin content in response to tolbutamide (F, n=5 saline/2.8 mM, n=4 saline/20 mM, n=5/group NAFL EV, $P=0.820$), diazoxide (G, n=6/group, $P=0.004$ (main effect)), arginine (H, n=6 saline/2.8 mM, n=5 saline/20 mM, n=6/group NAFL EV, $P=0.744$), alanine (I, n=9 saline/2.8 mM, n=11 saline/20 mM, n=11/group NAFL EV, $P=0.543$), and exendin 4 (J, n=5/group, $P=0.720$).

Data are expressed as mean ± SEM. Data was analysed using two-way repeated measures ANOVA (A, B, C, D, E, H, J) or two-way ANOVA (F, G, I) with Student Newman Keuls post-hoc analyses.

Extended data Table 1. Patient clinical variables.

Variable	No NAFLD (n=8)	NAFL (n=8)	NASH (n=3)	*P* value
Age	34.8 ± 9.6	42.5 ± 7.7	48.7 ± 8.1	0.08
Weight	124.8 ± 22.6	123.8 ± 17.6	106.2 ± 7.7	0.298
Sex (male %)	0	25	0	
Type 2 diabetes	0	0	0	
Alanine aminotransferase, IU/L	25.4 ± 12.2	47.6 ± 26.3	50.3 ± 11.6	0.086
Bilirubin, mmol/L	7.4 ± 2.1	8.1 ± 3.6	5.0 ± 1.7	0.293
Triglycerides, mmol/L	1.5 ± 1.1	1.3 ± 0.5	1.9 ± 0.4	0.315
Fasting blood glucose, mmol/L	4.8 ± 0.7	5.6 ± 2.8	5.2 ± 0.4	0.585
HOMA-IR	2.3 ± 1.6	3.2 ± 2.7	5.0 ± 0.8	0.201
Histology				
Steatosis (histology)				<0.001
S0 (<5%)	8 (100%)	0 (0%)	0 (0%)	
S1 (5-33%)	0 (0%)	7 (87.5%)	0 (0%)	
S2 (34-66%)	0 (0%)	1 (12.5%)	1 (33.3%)	
S3 (≥67%)	0 (0%)	0 (0%)	2 (66.7%)	
Inflammation				<0.05
0	8 (100%)	4 (50%)	0 (0%)	
1	0 (0%)	4 (50%)	2 (66.7%)	
2	0 (0%)	0(0%)	1 (33.3%)	
Ballooning				<0.001
0	8 (100%)	8 (100%)	0 (0%)	
1	0 (0%)	0 (0%)	2 (66.7%)	
2	0 (0%)	0 (0%)	1 (33.3%)	
NAFLD activity score (NAS)				<0.001
Not NASH (≤2)	8 (100%)	7 (87.5%)	0 (0%)	
Equivocal (3-4)	0 (0%)	1 (12.5%)	1 (33.3%)	
NASH (≥5)	0 (0%)	0 (0%)	2 (66.7%)	
Fibrosis				0.038
F0	3 (37.5%)	0 (0%)	0 (0%)	
F1	4 (50%)	6 (75%)	1 (33.3%)	
F2	1 (12.5%)	2 (25%)	1 (33.3%)	
F3	0 (0%)	0 (0%)	1 (33.3%)	
F4	0 (0%)	0 (0%)	0 (0%)	

Extended data Table 1. Patient clinical variables.

Extended data Table 1

NAFLD, non-alcoholic fatty liver disease; NAFL, non-alcoholic fatty liver; NASH, non-alcoholic steatohepatitis. Data is expressed as mean ± standard deviation and analysed using one-way ANOVA and Student-Newman-Keuls post-hoc analyses or Kruskal Wallis ANOVA on ranks with a Dunn's test. $P < 0.05$, indicated within table. For steatosis and NAS score: NAFL and NASH are significantly different than no NAFLD. Inflammation and fibrosis: NASH is significantly greater than no NAFLD. Ballooning: NASH is significantly greater than NAFL and no NAFLD.

Extended data Table. 2. Primer sequences

Primer	Supplier	Sequence
F4/80 forward	Merck	CCTGGACGAATCCTGTGAAG
F4/40 reverse	Merck	GGTGGGACCACAGAGAGTTG
Il-6 forward	Merck	CCAGTTTGCCTTCTTCCCACT
Il-6 reverse	Merck	GGTCTGTTGGGAGTGGTATCC
TGF-1β forward	Merck	GGATACCAACTATTGCTTCAG
TGF-1β reverse	Merck	TGTCCAGGCTCCAAATATAG
Col1a1 forward	Merck	CGTATCACCAAACTCAGAAG
Col1a1 reverse	Merck	GAAGCAAAGTTTCCTCCAAG
Cd11 forward	Merck	ATGGAGCCTCAAGACAGGAC
Cd11 reverse	Merck	GGATCTGGGATGCTGAAATC
Ctgf forward	Merck	GAGGAAAACATTAAGAAGGGC
Ctgf reverse	Merck	AGAAAGCTCAAACTTGACAG
Hprt forward	Merck	AGGGATTTGAATCACGTTTG
Hprt reverse	Merck	TTTACTGGCAACATCAACAG

nature portfolio

Corresponding author(s): Matthew Watt

Last updated by author(s): Dec 19, 2023

Reporting Summary

Nature Portfolio wishes to improve the reproducibility of the work that we publish. This form provides structure for consistency and transparency in reporting. For further information on Nature Portfolio policies, see our Editorial Policies and the Editorial Policy Checklist.

Statistics

For all statistical analyses, confirm that the following items are present in the figure legend, table legend, main text, or Methods section.

n/a	Confirmed	
☐	☒	The exact sample size (*n*) for each experimental group/condition, given as a discrete number and unit of measurement
☐	☒	A statement on whether measurements were taken from distinct samples or whether the same sample was measured repeatedly
☐	☒	The statistical test(s) used AND whether they are one- or two-sided *Only common tests should be described solely by name; describe more complex techniques in the Methods section.*
☒	☐	A description of all covariates tested
☐	☒	A description of any assumptions or corrections, such as tests of normality and adjustment for multiple comparisons
☐	☒	A full description of the statistical parameters including central tendency (e.g. means) or other basic estimates (e.g. regression coefficient) AND variation (e.g. standard deviation) or associated estimates of uncertainty (e.g. confidence intervals)
☐	☒	For null hypothesis testing, the test statistic (e.g. *F*, *t*, *r*) with confidence intervals, effect sizes, degrees of freedom and *P* value noted *Give P values as exact values whenever suitable.*
☒	☐	For Bayesian analysis, information on the choice of priors and Markov chain Monte Carlo settings
☒	☐	For hierarchical and complex designs, identification of the appropriate level for tests and full reporting of outcomes
☒	☐	Estimates of effect sizes (e.g. Cohen's *d*, Pearson's *r*), indicating how they were calculated

Our web collection on statistics for biologists contains articles on many of the points above.

Software and code

Policy information about availability of computer code

Data collection	Gene expression data was determined using CFX connect Real-time PCR. Cryo-electron microscopy was measured using a 300 kv Technai G2 F30 system. Nanoparticle tracking analyses were measured using a Zetaview PMX-120 analyser. Proteomic data was collected using an Orbitrap Elite mass spectrometer. ATP/ADP concentrations were determined using LC-MS on a QTRAP® 5500 mass spectrometer (AB-SCIEX). Flow cytometry data was measured using AMNIS Imagestream X MkII Imaging Flow Cytometer (AMNIS/Millipore). Whole body calorimetry was determined using a Promethium (Sable Systems Instruments).
Data analysis	Nanoparticle tracking analysis was analysed using Zetaview analyser software (version 8.05.12). Proteomic data was analysed using MaxQuant software (version 1.4.10.0 or 2.4.10.0) and Perseus (version 1.6.0.7). Phosphoproteomic data was analysed using Perseus and Spectronaut software. Pathways enrichment analysis was performed using Metascape (https://metascape.org/) and Ingenuity Pathways analysis (https://digitalinsights.qiagen.com). Flow cytometry data was analysed using AMNIS IDEAS® software. Area under the curve for glucose tolerance testing was calculated using GraphPad Prism software (version 9.4.1). Statistical analysis was conducted using SigmaPlot 11 software (build 11.2.0.5).

For manuscripts utilizing custom algorithms or software that are central to the research but not yet described in published literature, software must be made available to editors and reviewers. We strongly encourage code deposition in a community repository (e.g. GitHub). See the Nature Portfolio guidelines for submitting code & software for further information.

Data

Policy information about availability of data

All manuscripts must include a data availability statement. This statement should provide the following information, where applicable:

- Accession codes, unique identifiers, or web links for publicly available datasets
- A description of any restrictions on data availability
- For clinical datasets or third party data, please ensure that the statement adheres to our policy

All data is available within the manuscript, extended data, source data files, and supplemental files. The analysis in this study has used standard techniques and protocols without generating new unique reagents or custom code. The proteomic and phosphoproteomic data generated in this study are deposited to the ProteomeXchange Consortium (http://proteomecentral.proteomexchange.org/cgi/GetDataset) via the PRIDE 84, under the identifiers PXD037924, PXD036400, and PXD043137. These data are also provided as supplemental information.

Research involving human participants, their data, or biological material

Policy information about studies with human participants or human data. See also policy information about sex, gender (identity/presentation), and sexual orientation and race, ethnicity and racism.

Reporting on sex and gender	Biological sex: 17 female and 2 male participants undergoing bariatric surgery consented to take part in the study.
Reporting on race, ethnicity, or other socially relevant groupings	Information regarding race, ethnicity, or other socially relevant groupings were not collected in this study. This was a prospective study.
Population characteristics	Patients undergoing bariatric surgery ranged from age 24-56 (17 female, 2 male), and were subsequently characterized with normal liver, non-alcoholic fatty liver disease, or non-alcoholic steatohepatitis based on liver sectioning, staining with hematoxylin and eosin or Masson's Trichrome, and scoring by an expierienced histopathologist in a blinded manner in accordance with the Clinical Research Network NAFLD activity score (NAS).
Recruitment	In this prospective cohort study, obese patients undergoing bariatric surgery consented in writing. Exclusion criteria involved: <18 year of age, excessive alcohol use, evidence of other liver disease including viral hepatitis, cirrhosis, autoimmune hepatitis, and hyperthyroidism. Clinical details including metabolic comorbidities, body weight, height, medications, and medical history were collected using a questionnaire, and fasting blood was collected for the measurement of ALT. A 1 cm3 wedge biopsy was collected, and precision cut liver slices were prepared for subsequent analyses. Data were grouped based on unbiased liver pathology, assessed in a blinded manner.
Ethics oversight	Collection of human tissues were done in accordance with human ethics at the University of Melbourne (ID 1851533) and approved by The Avenue Hospital Human Research Ethics Committee (ID WD00006) and the Alfred Hospital Human Research Ethics Committee (ID GO00005).

Note that full information on the approval of the study protocol must also be provided in the manuscript.

Field-specific reporting

Please select the one below that is the best fit for your research. If you are not sure, read the appropriate sections before making your selection.

☒ Life sciences ☐ Behavioural & social sciences ☐ Ecological, evolutionary & environmental sciences

For a reference copy of the document with all sections, see nature.com/documents/nr-reporting-summary-flat.pdf

Life sciences study design

All studies must disclose on these points even when the disclosure is negative.

Sample size	Sample size was determined based on previously published papers containing similar methods and data from our lab using these protocols. The sample size pertaining to specific experiments is indicated in the figure legends.
Data exclusions	Statistical analysis was used to identify outliers to be removed from analyses. Data points derived from failed experiments were not included.
Replication	Certain outcomes were repeated regularly throughout the study across independent cohorts (i.e., glucose tolerance testing in response to liver extracellular vesicles). Experiments display at least 3 replicates and are described in the figure legends.
Randomization	Mice of the same age and similar body weight were randomly selected to receive either a control, high-fat (40%, NAFL) or high-fat + high-fructose + 2% cholesterol diet (NASH) for 20 weeks. Saline or extracellular vesicle injections were selected to be equal between mice of similar weight across conditions.

Blinding	Scoring of liver histology occurred in a blinded manner by an experience pathologist. The other experiments were not blinded due to the control of applying certain treatments to mice or cell culture experiments.

Reporting for specific materials, systems and methods

We require information from authors about some types of materials, experimental systems and methods used in many studies. Here, indicate whether each material, system or method listed is relevant to your study. If you are not sure if a list item applies to your research, read the appropriate section before selecting a response.

Materials & experimental systems

n/a	Involved in the study
☐	☒ Antibodies
☐	☒ Eukaryotic cell lines
☒	☐ Palaeontology and archaeology
☐	☒ Animals and other organisms
☒	☐ Clinical data
☒	☐ Dual use research of concern
☒	☐ Plants

Methods

n/a	Involved in the study
☒	☐ ChIP-seq
☐	☒ Flow cytometry
☒	☐ MRI-based neuroimaging

Antibodies

Antibodies used	For western blotting: Anti-TSG-101 (1:1000, Abcam, cat# ab125011; RRID: AB_10974262), Anti-CD63 (1:1000, Abcam, cat#CD63; RRID: AB_2800495), Anti-CD81 (1:1000, Abcam, cat# ab109201; RRID: AB_10866464), Anti-calnexin (1:1000, Abcam, cat# ab133615; RRID: AB_2864299), CD9 (1:1000, Abcam, Cat# ab263019), HSP70 (1:1000, Abcam, Cat# ab181606; RRID:AB_2910093), GLUT4 (1:1000, Abcam Cat# ab33780, RRID:AB_2191441), CAV3 (1:1000, Abcam Cat# ab2912, RRID:AB_2291095). Anti-rabbit secondary antibody (Cytiva, Cat# NA934V)was used at a 1:2000 dilution. For flow cytometry: Anti-CD63-PE-Cy7 (0.5µg/20µl, Thermo Fisher, Clone NVG-2, Cat# 25-0631-82; RRID: AB_2573356), Anti-CD9-APC (0.5µg/20µl, BioLegend, Clone MZ3, Cat# 124812; RRID: AB_2783071), Anti-ASGPR1-PE (2.5µl/20µl, BD Biosciences, Clone 8D7, Cat# 563655; RRID: AB_2687910), PE Mouse IgG1 Kappa isotype control (2.5µl/20µl, BD Biosciences, Cat# 551436; RRID: AB_394195) .
Validation	Antibodies have been previously validated by commercial suppliers and published papers (Peters et al. 2016, Development). In the current study, these antibodies were validated by the enrichment of extracellular vesicle-specific proteins in extracellular vesicle samples compared to whole tissue lysates, as well as the absence of contaminants in the extracellular vesicle sample preparation.

Eukaryotic cell lines

Policy information about cell lines and Sex and Gender in Research

Cell line source(s)	C2C12 (ATCC, CRL_1772). Primary pancreatic islets and hepatocytes were isolated from male C57BL6J mice.
Authentication	The validity of isolated hepatocytes has been previously shown in our laboratory (Meex et al. 2015, Cell Metab). The purity of the islets has been previously validated by our collaborators (Yang, et al., 2022, Mol Metab). C2C12 differentiation was confirmed using bright-field microscopy, and treatments were evenly allocated. Positive controls in the non-extracellular vesicle treated condition for each cell type were determined by glucose-stimulated glucose uptake and insulin-stimulated AKT phosphorylation (C2C12), glucose-stimulated insulin secretion and an increased ATP/ADP ratio (primary islets), and insulin-mediated suppression of hepatic glucose output (hepatocytes).
Mycoplasma contamination	Cells were not tested for mycoplasma contamination in the current study.
Commonly misidentified lines (See ICLAC register)	No commonly misidentified lines are used in the current study.

Animals and other research organisms

Policy information about studies involving animals; ARRIVE guidelines recommended for reporting animal research, and Sex and Gender in Research

Laboratory animals	Male C57BL6J (Australian Resource Centre; JAX000664) and NOD/SCID (Animal Resource Centre; JAX001303) mice. Mice were group housed in the Biomedical Science Animal Facility (BSAF) at the University of Melbourne, on a 12 hr:12 hr light/dark cycle at 22-24 °C and 40-60% humidity, with free access to food and water. n sizes for each experiment is provided in the figure legends.

Wild animals	This study did not use wild animals.
Reporting on sex	Male mice were used in the present study due to their consistent responsiveness to the diets used to induce progressive fatty liver disease. n sizes for each experiment are described in the figure legends.
Field-collected samples	This study did not use field-collected samples.
Ethics oversight	All animal procedures were done in accordance with the guidelines for the care and use of laboratory animals and approved by the Animal Welfare and Ethics Committee at the University of Melbourne (AEC 1814403, 1814363, 20063, 22305).

Note that full information on the approval of the study protocol must also be provided in the manuscript.

Plants

Seed stocks	N/A
Novel plant genotypes	N/A
Authentication	N/A

Flow Cytometry

Plots

Confirm that:

☒ The axis labels state the marker and fluorochrome used (e.g. CD4-FITC).

☒ The axis scales are clearly visible. Include numbers along axes only for bottom left plot of group (a 'group' is an analysis of identical markers).

☒ All plots are contour plots with outliers or pseudocolor plots.

☒ A numerical value for number of cells or percentage (with statistics) is provided.

Methodology

Sample preparation	Isolated serum EV were incubated in 20 µl of filtered 0.2% BSA in PBS (BSA-PBS solution) containing 0.5 µg CD63-PE-Cy7 (Thermo Fisher, Cat# 25-06-31-82), 0.5 µg CD9-APC (Bio Legend, Cat# 124812), and 2.5 µl ASGPR1-PE (BD Biosciences, Cat# 563655) or PE Mouse IgG1 Kappa isotype control (BD Biosciences, Cat# 551436) for 1 hour in the dark at room temperature. EVs were then diluted to 1 ml before spun at 100,000 x g for 1 hour. Pellets were then reconstituted in BSA-PBS solution.
Instrument	AMNIS Imagestream X MkII Imaging Flow Cytometer (AMNIS/Millipore).
Software	AMNIS IDEAS® software.
Cell population abundance	Serum EVs were analysed using 60x objective at a low flow rate with the sample acquisition cut-off set to 5,000 events.
Gating strategy	First, all events were gated based on the brightfield signals using the Gradient RMS feature to remove any acquired signals that were not in focus. Then, the aspect ratio was plotted against the area of acquired particles to discriminate EV and speed beads (previously optimised). Particles with an area smaller than the speed beads were gated. Fluorescence signals from Ch06 were then plotted against Ch11 to identify the double positive population. The Ch03 signals were plotted on a histogram and gated based on the isotype control.

☒ Tick this box to confirm that a figure exemplifying the gating strategy is provided in the Supplementary Information.